Distributed fiber sensing systems for 3D combustion temperature field monitoring in coal-fired boilers using optically generated acoustic waves
(DE-FE0023031)

Project manager: Jessica Mullen, Barbara Carney

PIs: Xingwei (Vivian) Wang[1], Chengyu Cao[2], and Xinsheng Lou[3]

University of Massachusetts Lowell[1]
University of Connecticut[2]
General Electric Power[3]

Advantages

- Combination of the advantages of
  - Optical fiber sensing:
    - Distributed sensing;
    - Survivability in harsh environments:
    - Immunity to electromagnetic interference
  - Acoustic sensing:
    - Noncontact approach
    - Penetration depth
- Other applications:
  - Corrosion monitoring
  - Imaging

Patent Application and Optioning

Patent application:

- 2016 Xingwei Wang, Nan Wu, "Photoacoustic Probe", WO2016178981 A1, WO2012112890A2; EP2675361A2; US20130319123A1; WO2012112890A3.
- PCT nationalization coming up in November, 2017.
- One company is interested in optioning UML 15-32 IP and explore its commercialization.

Outline

- Brief overview of DOE project
- Sensing system development
- Signal processing
- Temperature reconstruction algorithm
- Conclusions & Future work

Introduction

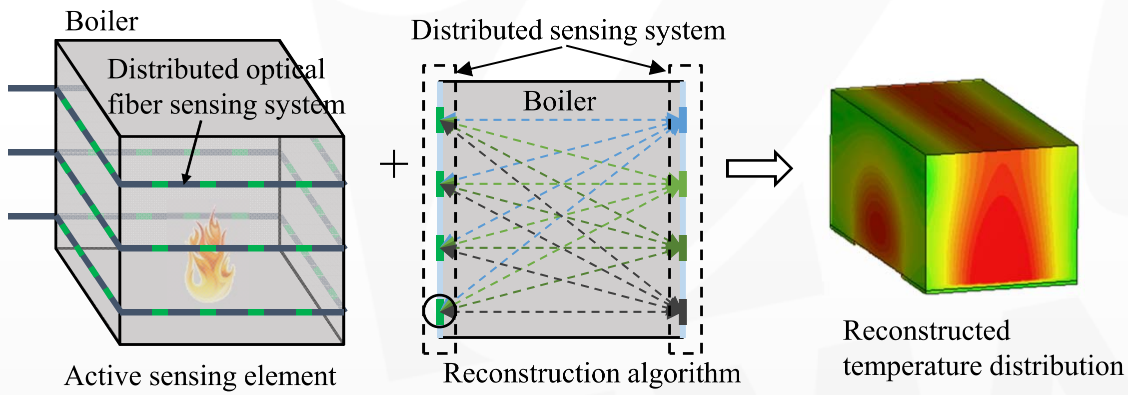

Overview of DOE project.

- Reconstruct the 3D high temperature distribution within a boiler with a novel fiber optic distributed temperature sensing system that uses optically generated acoustic waves.

Introduction

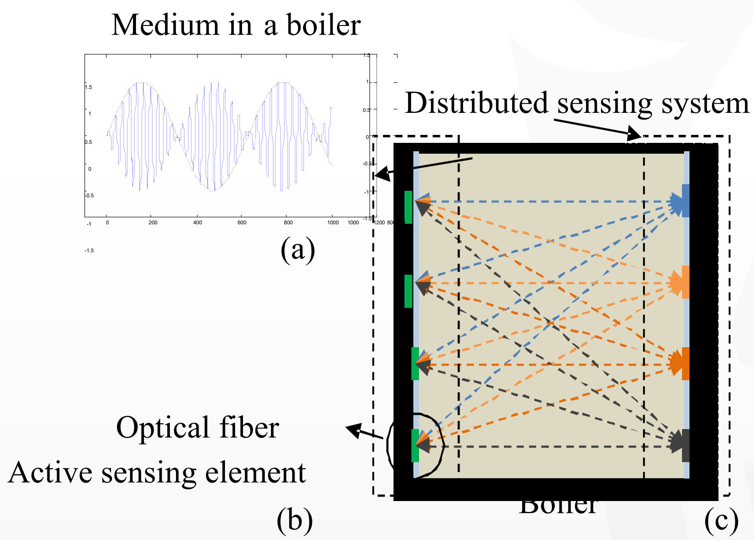

Principle of DOE project.

❑ Speed of acoustic waves depend on the temperature of gaseous medium.

❑ The TOF (time-of-flight) of an acoustic signal over a propagation path can be calculated as:

$$TOF(l_j) = \int \frac{1}{C(x,y,z)} dl_j = \int \frac{1}{Z\sqrt{T(x,y,z)}} dl_j$$

$C(x,y,z)$ the velocity of sound at position (x,y,z)

z the ratio between the specific heats at constant pressure and volume of the gas

$d(x,y,z)$ the reciprocal of velocity

j the number of paths;

Outline

- ❑ Brief overview of DOE project
- ❑ Sensing system development
  1. Photoacoustic generator
     - Principle
     - Tip generator
     - Sidewall generator
  2. Signal receiver
     - Fiber Bragg grating (FBG) fiber sensor
     - Fabry-Perot (F-P) fiber sensor
  3. Temperature measurement
     - Water temperature measurement
     - Steel plate temperature measurement
     - Air temperature test and reconstruction
  4. Distributed sensing capability test
  5. GE pilot test
  6. Furnace test
- ❑ Signal Processing
- ❑ Temperature reconstruction algorithm
- ❑ Conclusions

Photoacoustic

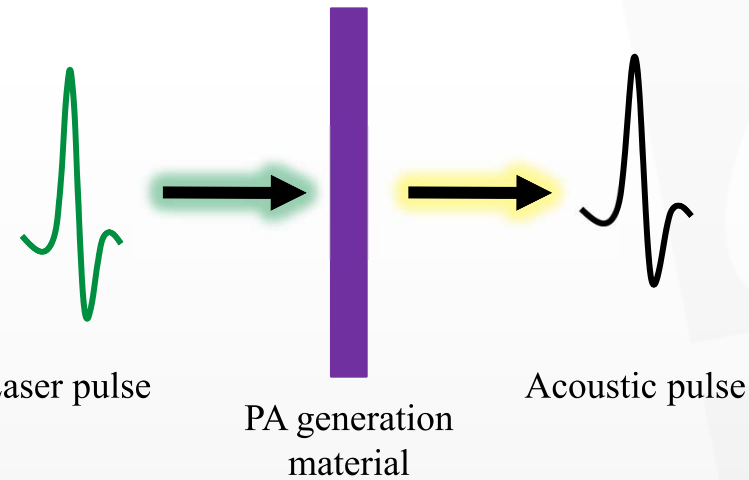

Photoacoustic definition

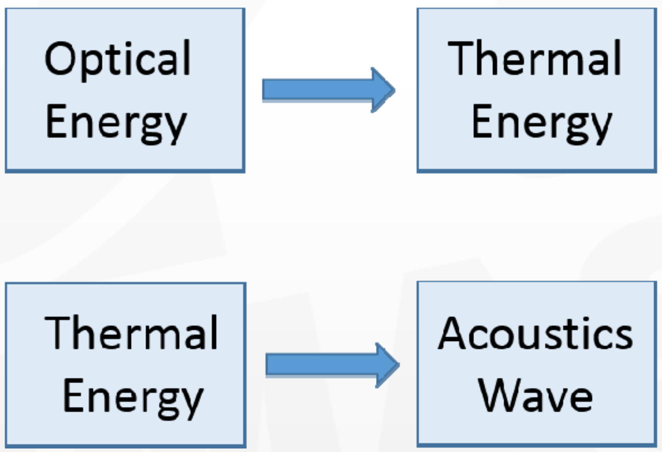

Photoacoustic principle

- Note: The PA principle is an optical approach to generate ultrasound signals [1, 2]. It involves a PA generation material which absorbs the optical energy from the laser and converts it into a rise in localized temperature.

Photoacoustic

Simulation of photoacoustic

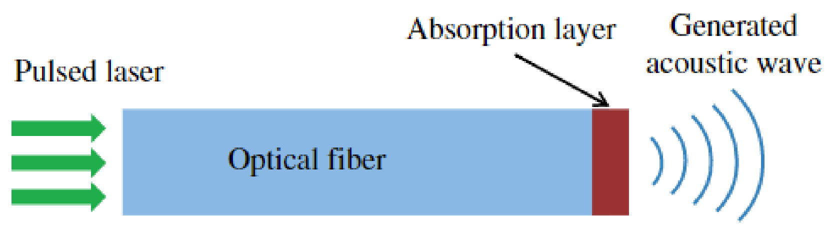

Schematic of a fiber-optic photoacoustic generator [3]

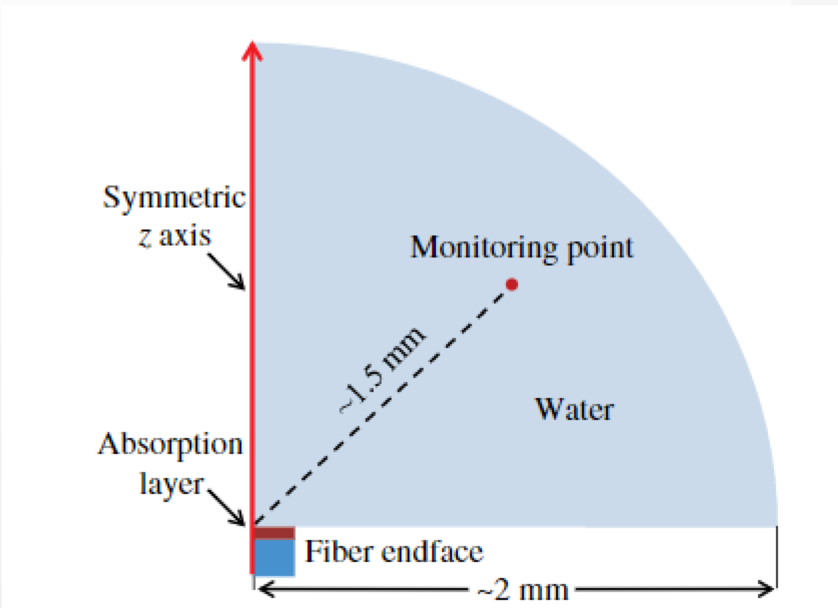

2D-axisymmetric FEA model of the photoacoustic generator

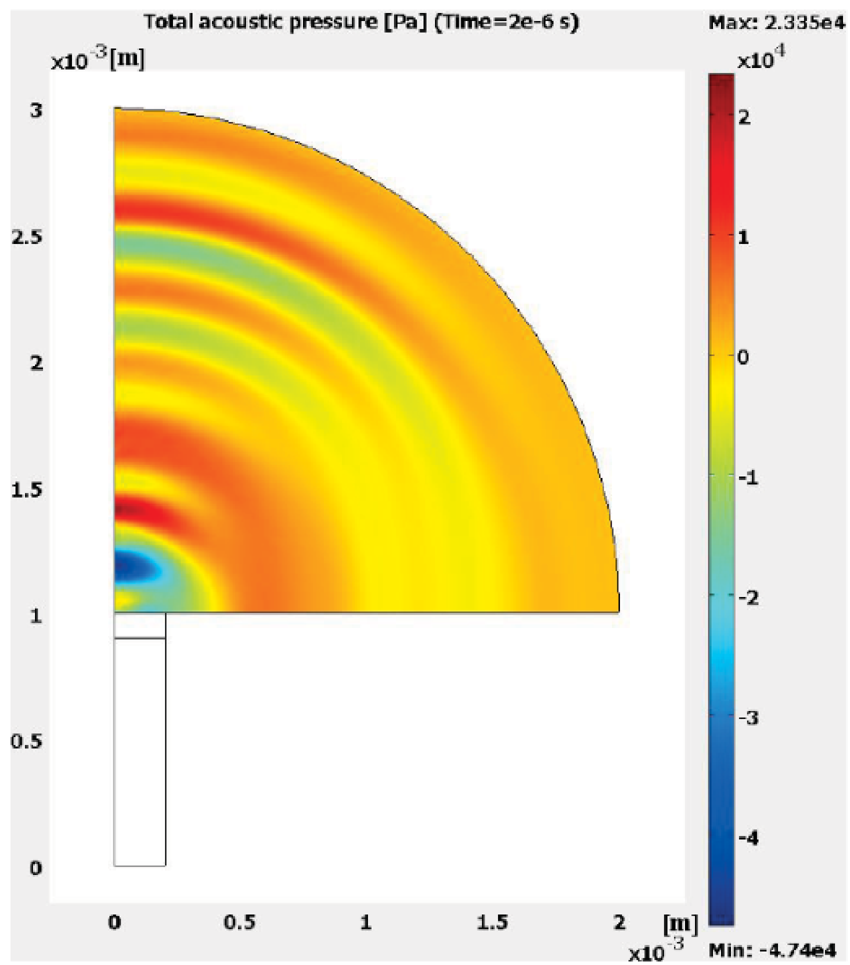

Acoustic pressure distribution at 2 μs generated by an absorption layer (100 μm thick)

Photoacoustic

Simulation of photoacoustic

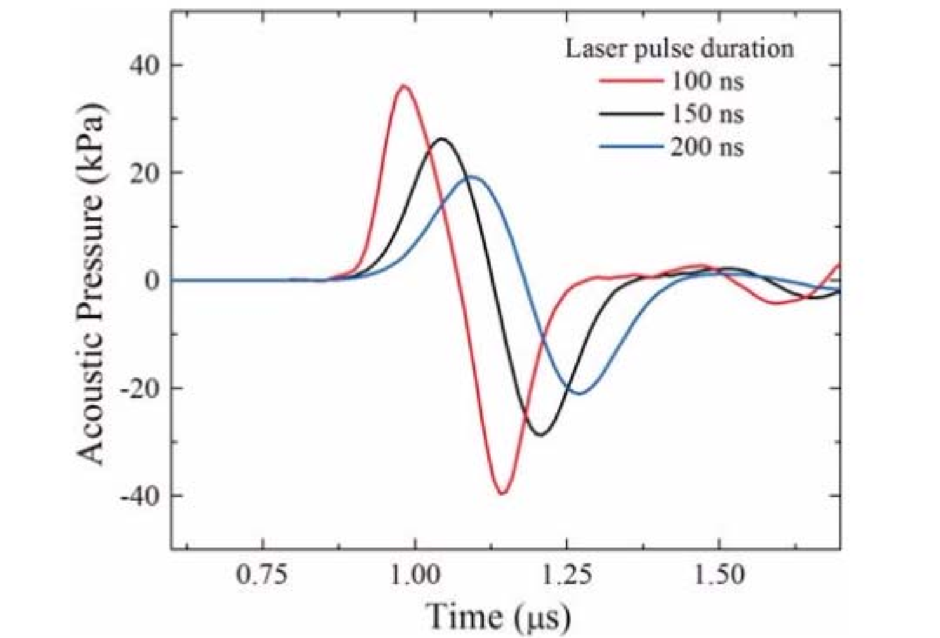

Acoustic pressure at the monitoring point for different laser pulse durations (100, 150, and 200 ns.)

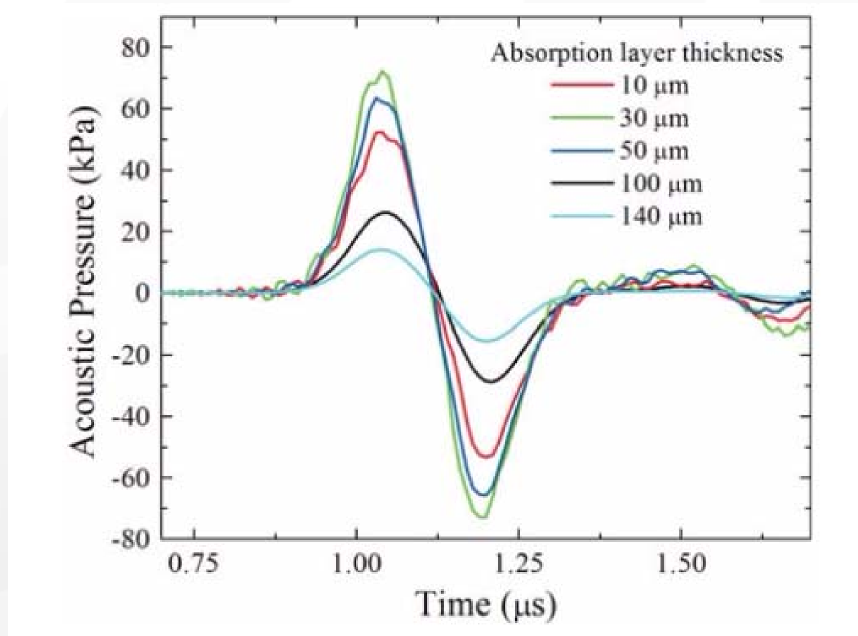

Acoustic pressure at the monitoring point for different layer thicknesses (10–140 μm)

Photoacoustic

Photoacoustic materials

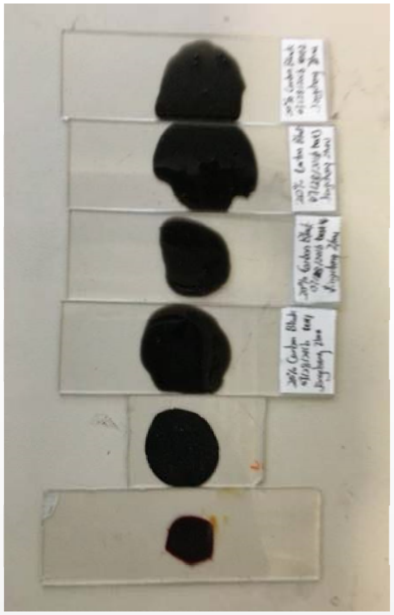

Carbon Black 1

Carbon Black 2

Carbon Black 3

Carbon Black 4

Carbon Black 5

Gold-nanocomposite

Different photoacoustic materials

Ultrasound signal strength generated by different photoacoustic materials

	First Test (mV)	Second Test (mV)	Third Test (mV)	Average (mV)
Carbon Black 1	3.0	3.0	2.8	2.93
Carbon Black 2	2.9	2.5	2.6	2.67
Carbon Black 3	2.2	2.2	2.4	2.27
Carbon Black 4	2.4	2.6	2.5	2.50
Carbon Black 5	2.1	2.1	2.2	2.13
Gold Nanocomposite	2.5	2.2	2.3	2.33

- Carbon Black 1-4 are 20% Carbon black (partial size 20 nm) + PDMS.
- Carbon Black 5 is 20% Carbon black (partial size 101 nm) + PDMS.
- Gold-nanocomposite is 12% Gold-nanoparticle + PDMS.
- Carbon Black 5 had the lowest ultrasound signal, due to it being used many times, which may have caused damage to it.
- Carbon Black 3 generated a low ultrasound signal because the thickness and the size of it was smaller than the others.

Tip generator

Photoacoustic materials coated on fiber tip

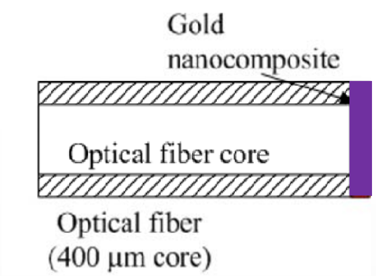

Structure of the tip generator

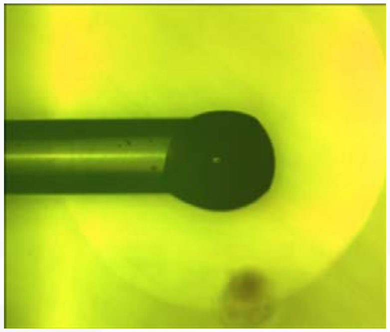

Microscope photo of the tip generator [1]

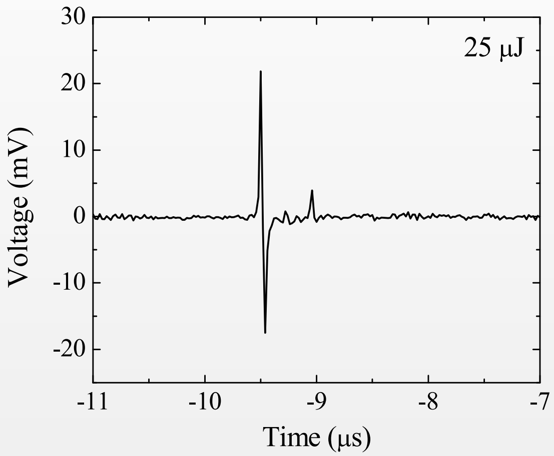

Profile of the generated ultrasound signal [2]

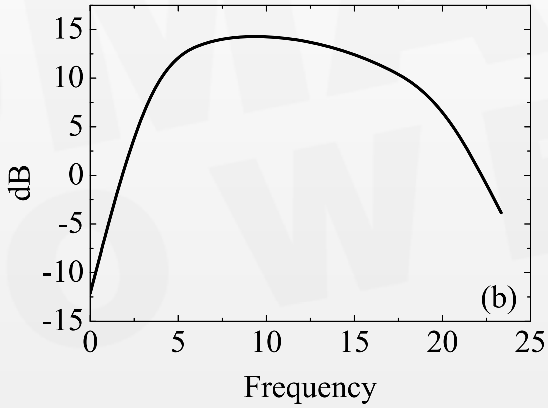

Bandwidth is wider than 20 MHz

Tip generator

Photoacoustic materials coated on glass slide

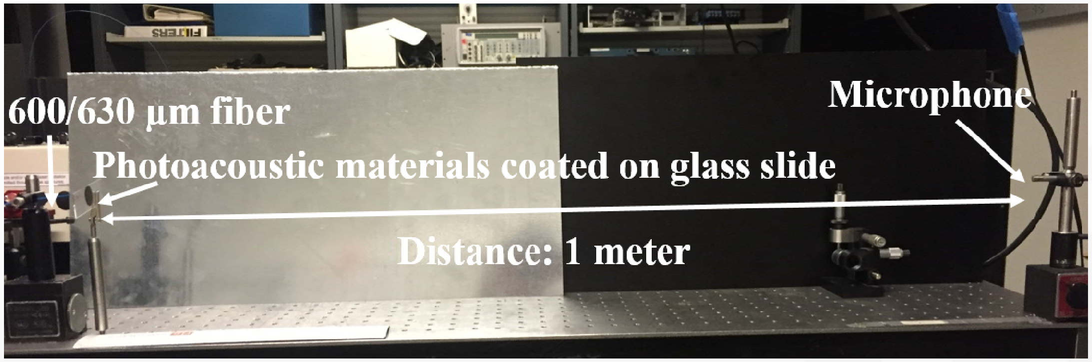

Experimental setup

◆ Note: This fiber optic ultrasound transducer system worked at a distance of 1 meter.

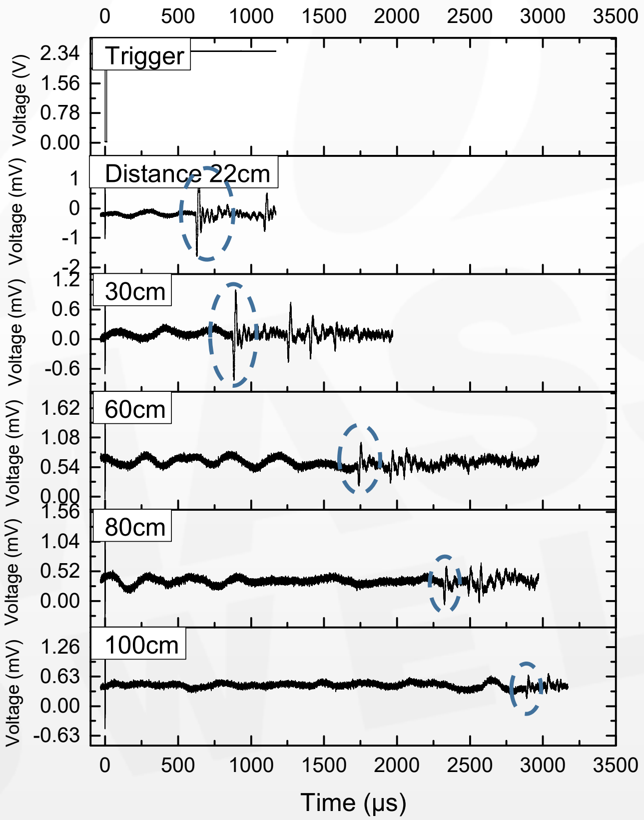

Ultrasound signals at different distances.

Sidewall generator

Sidewall configuration 1

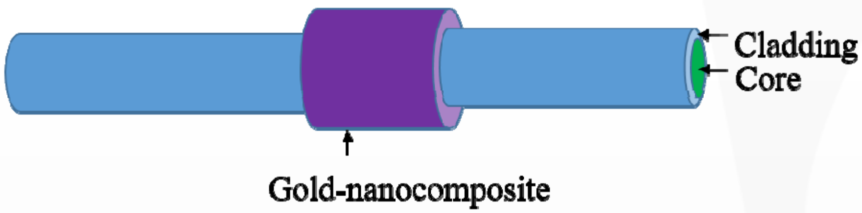

Coat gold nanocomposite on the sidewall of optical fibers [4].

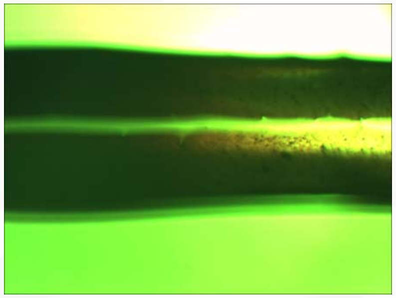

Sidewall ultrasound generator configuration 1.

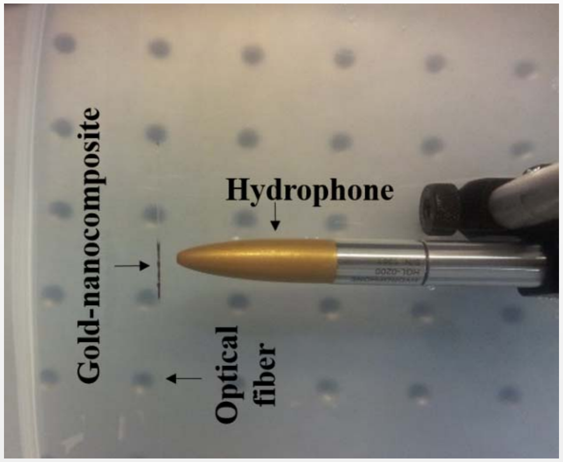

Experiment setup: test a sidewall generator.

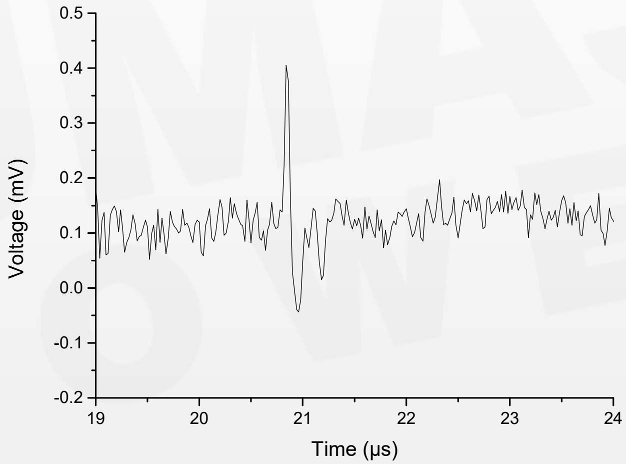

Acoustic signal generated from sidewall configuration 1.

- Note: Generated ultrasound signal was from the sidewall of a 400/425 µm fiber. A 532 nm Nd:YAG nanosecond laser (Surelite I-10, Continuum) was utilized as the optical radiation source. A hydrophone (HGL-0200, Onda) was used as a receiver to collect the ultrasound signals.

Sidewall generator

Sidewall configuration 2

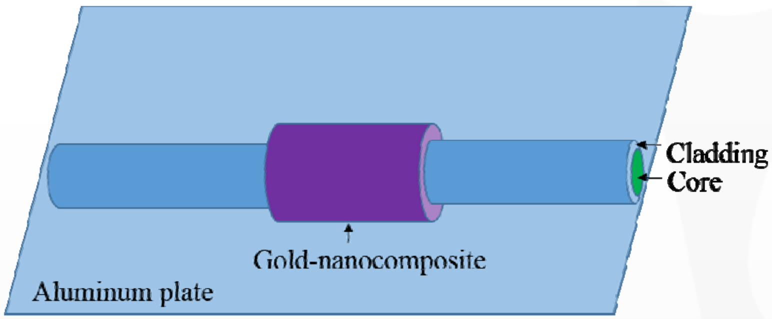

Sidewall fiber generator mounted on an aluminum plate [4].

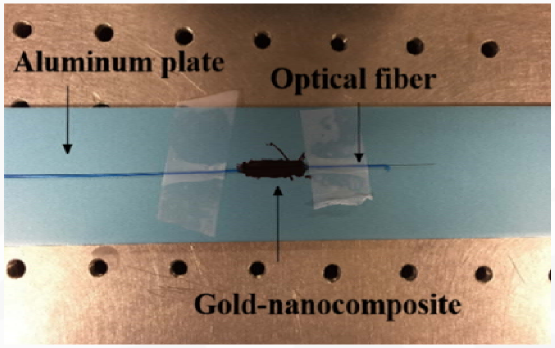

Sidewall ultrasound generator configuration 2.

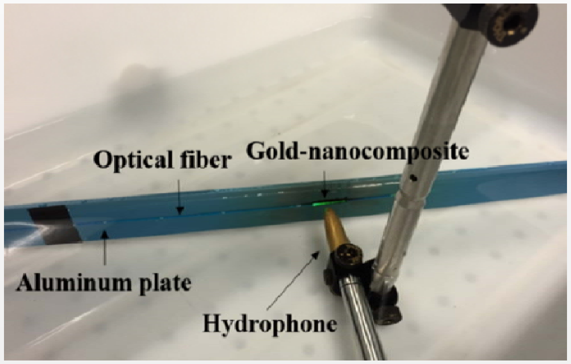

Experimental setup: test the sidewall ultrasound generator configuration 2.

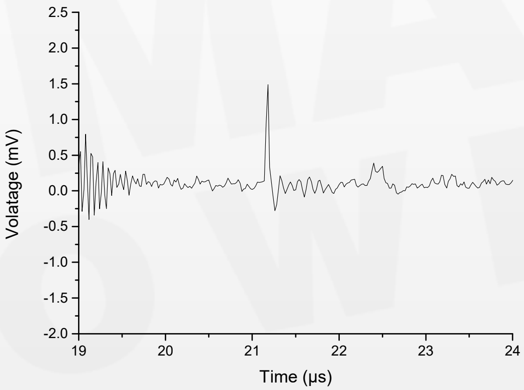

Acoustic signal generated from sidewall ultrasound generator configuration 2.

- Note: Ultrasound signal generated from this configuration on the aluminum plate was much higher than pervious configuration when the laser power and detection distance is the same.

Fiber Bragg Grating (FBG) fiber sensor

Fiber Bragg Grating performance comparison with hydrophone

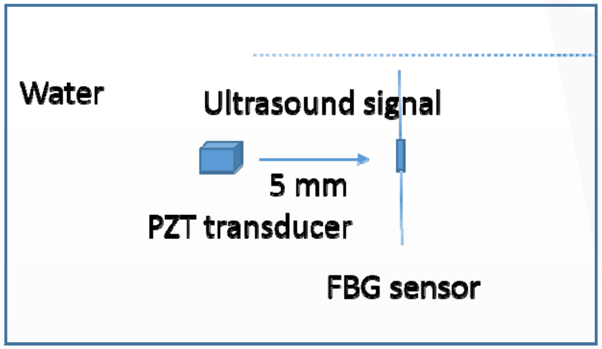

PZT as signal generator, FBG as signal receiver

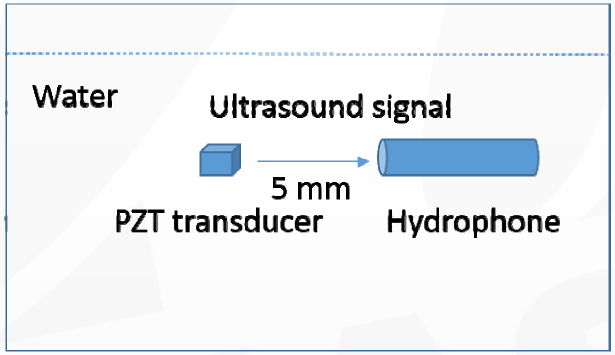

PZT as signal generator, Hydrophone as signal receiver

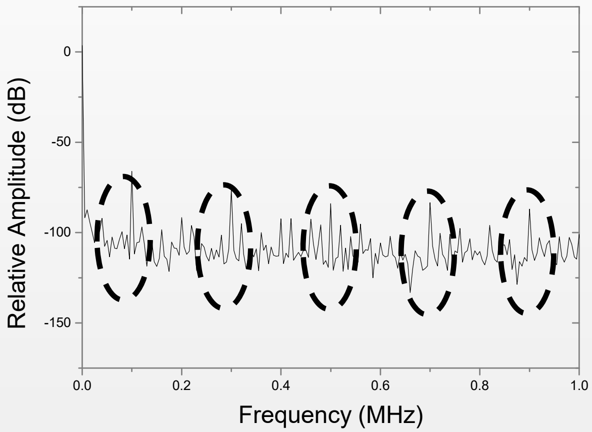

Ultrasound signal received by FBG in frequency domain

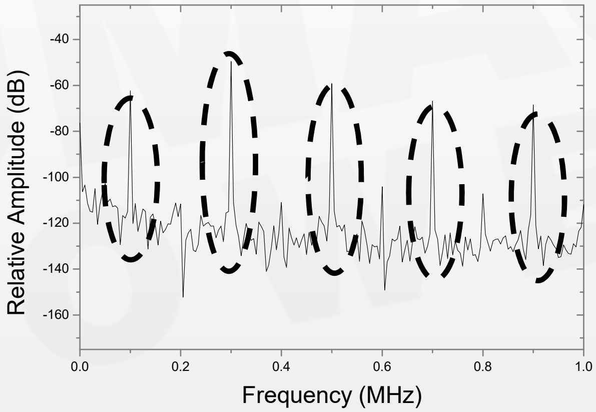

Ultrasound signal received by Hydrophone in frequency domain

- Note: FBG fiber sensor got same results as hydrophone in the frequency domain. It showed that the FBG fiber sensor could be used to detect the ultrasound signal in water.

Fabry-Perot (F-P) fiber sensor

F-P fiber sensor structure

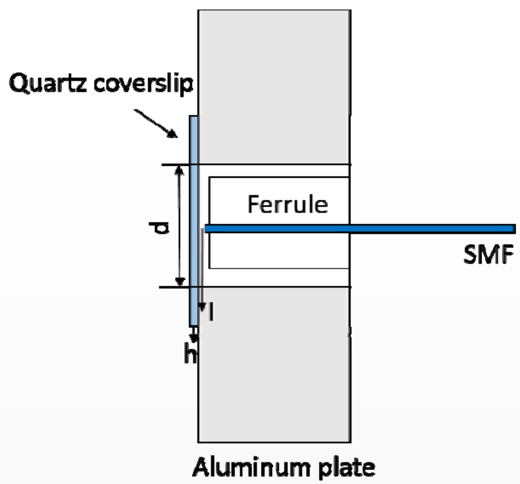

Structure of the F-P fiber sensor

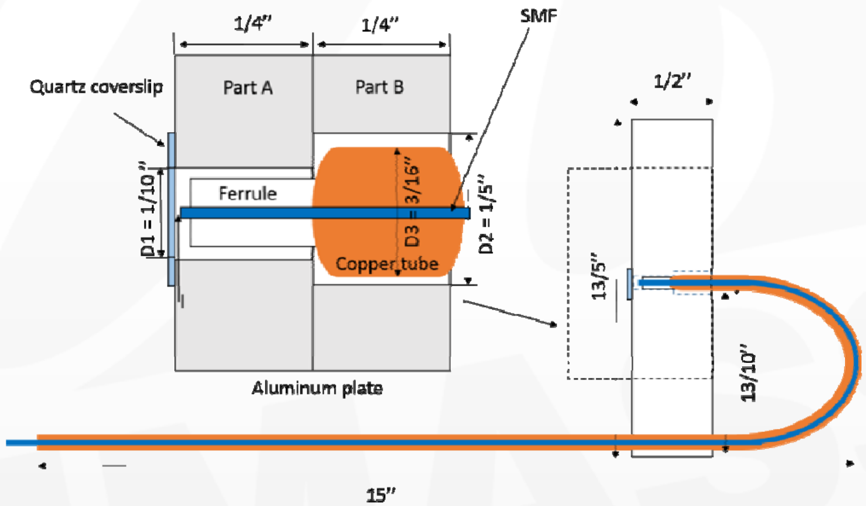

Packaging of the F-P fiber sensor

Sensitivity (How much the center of the diaphragm will be deformed when a certain acoustic pressure applied on it):

$$Y_c = \frac{3(1-\mu^2)(d/2)^4}{16Eh^3} \cdot 10^9 \ (nm/Pa)$$

E is the quartz's Young's modulus, $E = 7.2*10^{10}$ Pa;
μ is the quartz Poisson ratio, $\mu = 0.17$;
h is the thickness of the quartz coverslip, $h = 0.10$ mm;
d is the diameter of the aluminum hole, $d = 2.54$ mm;
$Y_c = 0.0032$ nm/Pa.

Resonant Frequency:

$$f_{00} = \frac{\alpha_{00}}{4\pi}[\frac{E}{3w(1-\mu^2)}]^{1/2}[\frac{h}{(d/2)^2}]\ Hz$$

f_{00} is the lowest resonant frequency;
α_{00} is a constant related to the vibrating modes, $\alpha_{00} = 10.21$;
w is the mass density of the quartz, $w = 2.50$ g/cm^3.
E is Young's modulus of quartz coverslip, $E = 7.20*10^{10}$ Pa;
μ is the Poisson ratio of quartz, $\mu = 0.17$;
h is the thickness of the diaphragm, $h=0.10$ mm;
d is the diameter of the diaphragm, $d=2.54$ mm.
f_{00} could be calculated as 1.8805e+05 Hz which is 0.19 MHz.

Fabry-Perot (F-P) fiber sensor

F-P fiber sensor performance comparison with microphone

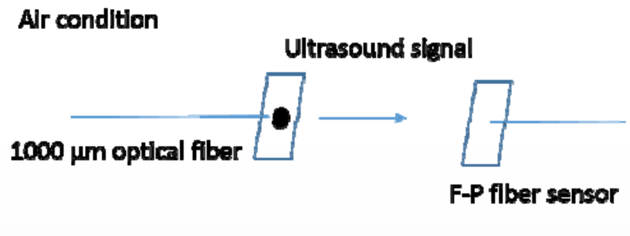

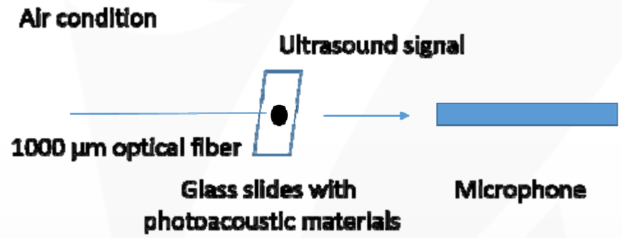

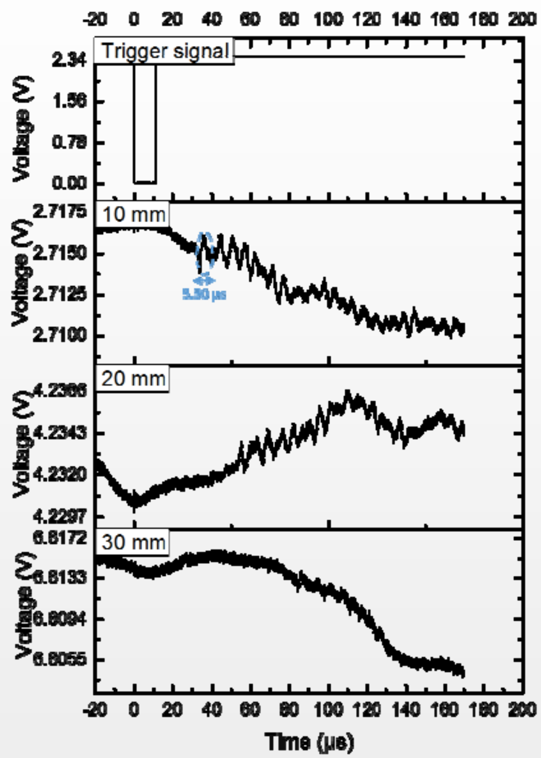

Ultrasound signal detected by F-P fiber sensor (V20161202TEST2)

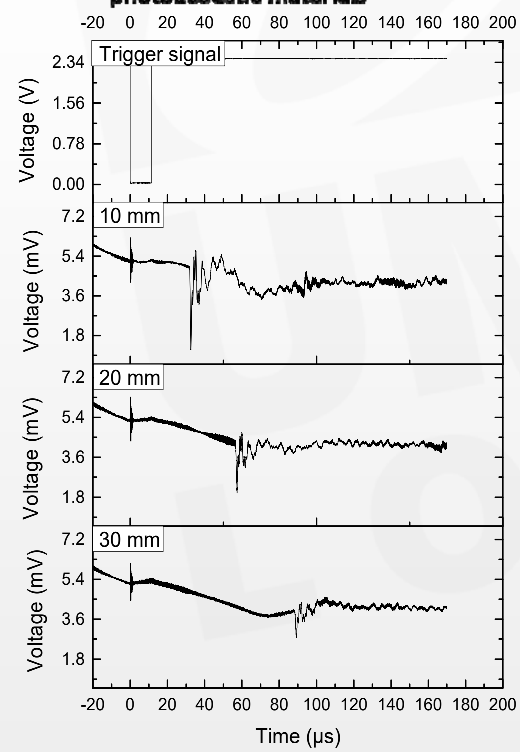

Ultrasound signal detected by PCB microphone

- At the distance of 10 mm, the Vpp from the microphone and the FP sensor was 4.50 mV and 2.23 mV, respectively.
- The F-P fiber sensor (V20161202TEST2) has half the sensitivity of the microphone.
- The sensitivity of the microphone is 22.51 mV/Pa. Therefore, the F-P fiber sensor is 11.25 mV/Pa.
- The time cycle of the ultrasound signal detected by the F-P fiber sensor is shown on the left Fig which was 5.50 μs.
- The frequency was calculated as: $\frac{1}{5.50\ \mu s} =$ 0.18 MHz.
- It was very close to 0.19 MHz, meaning it matched the resonant frequency calculation results.

Water temperature measurement

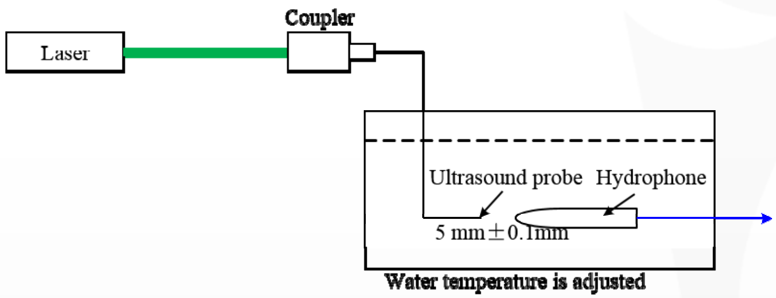

Schematic diagram of the water temperature measurement setup [1].

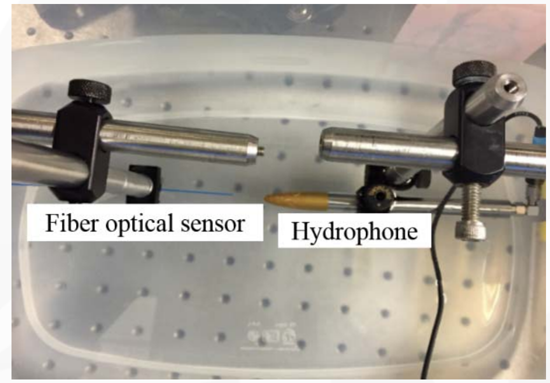

Photo of the water temperature measurement setup.

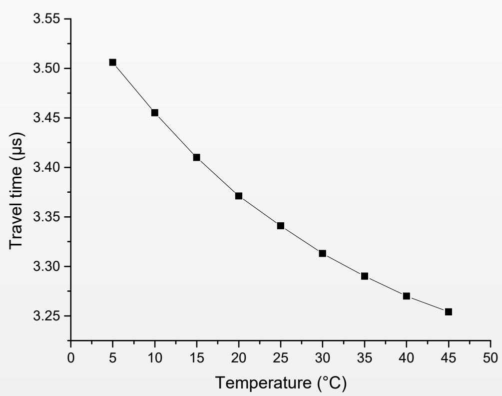

Travel time V.S. water temperature based on Marczak equation.

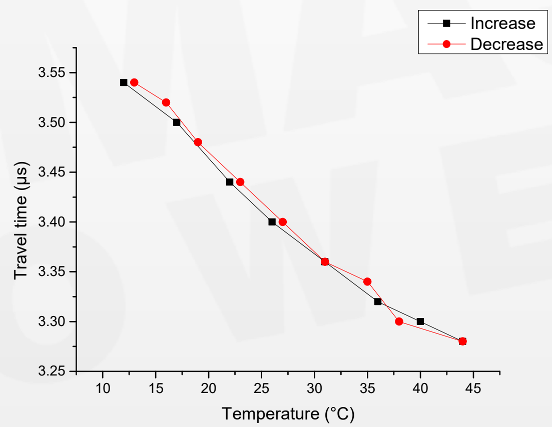

Experimental results: water temperature V.S. travel time

- Note: It demonstrated the temperature measurement capability of the fiber optic ultrasound transducer system in water.

Aluminum plate temperature measurement

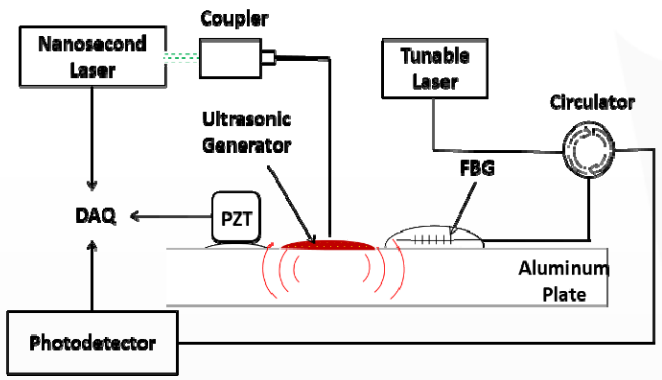

Schematic diagram of steel plate temperature measurement [5].

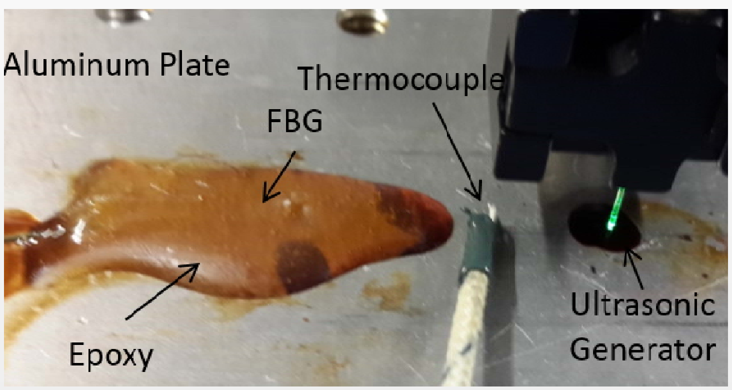

Photo of the Aluminum plate temperature measurement

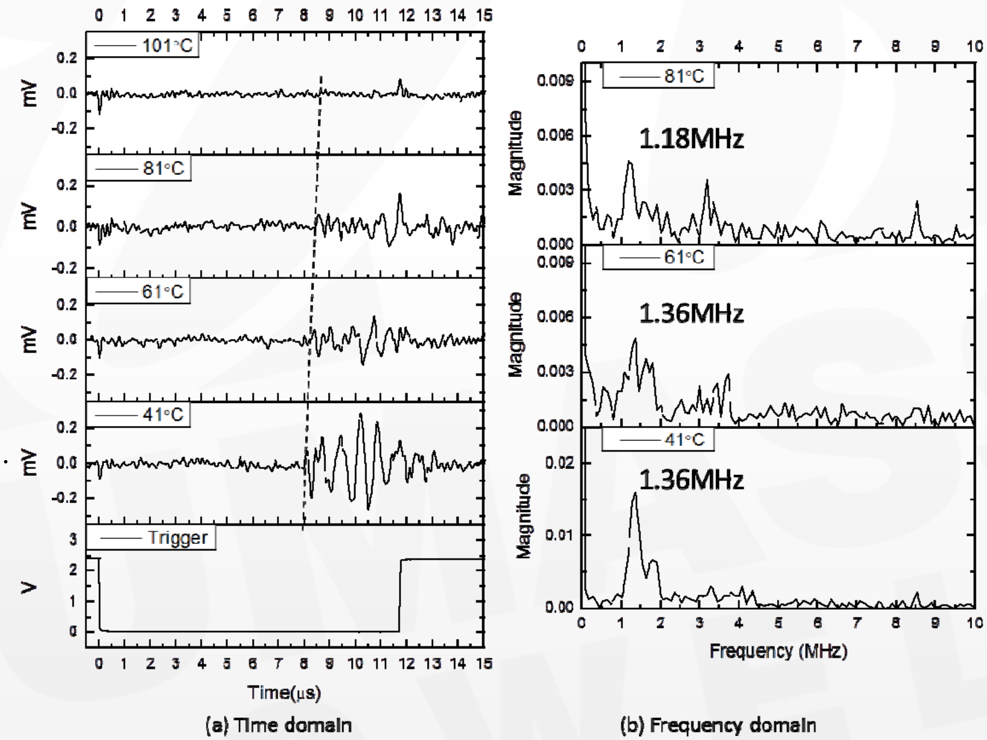

Experimental results of aluminum plate temperature test in (a) time domain and (b) frequency domain by FBG

- Note: FBG fiber sensor was used as the signal receiver in the solid condition. It proved the fiber optic ultrasound transducer system.

Air temperature test

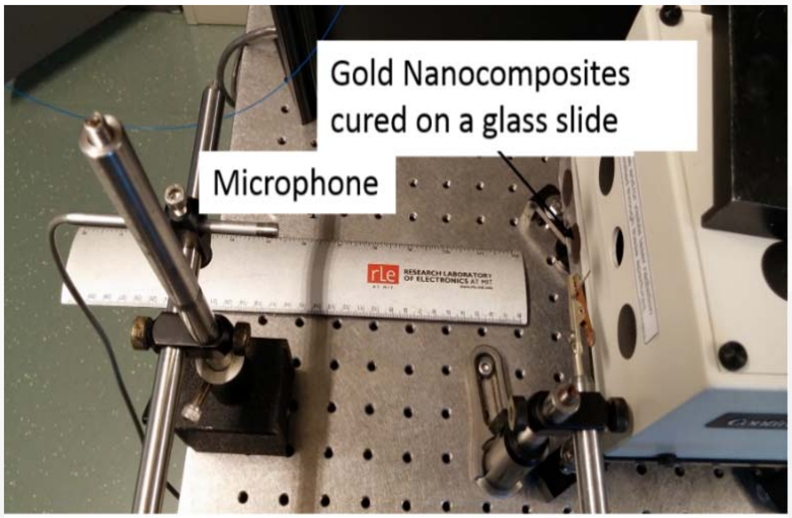

Experimental setup: Measure the temperature of a torch flame [4].

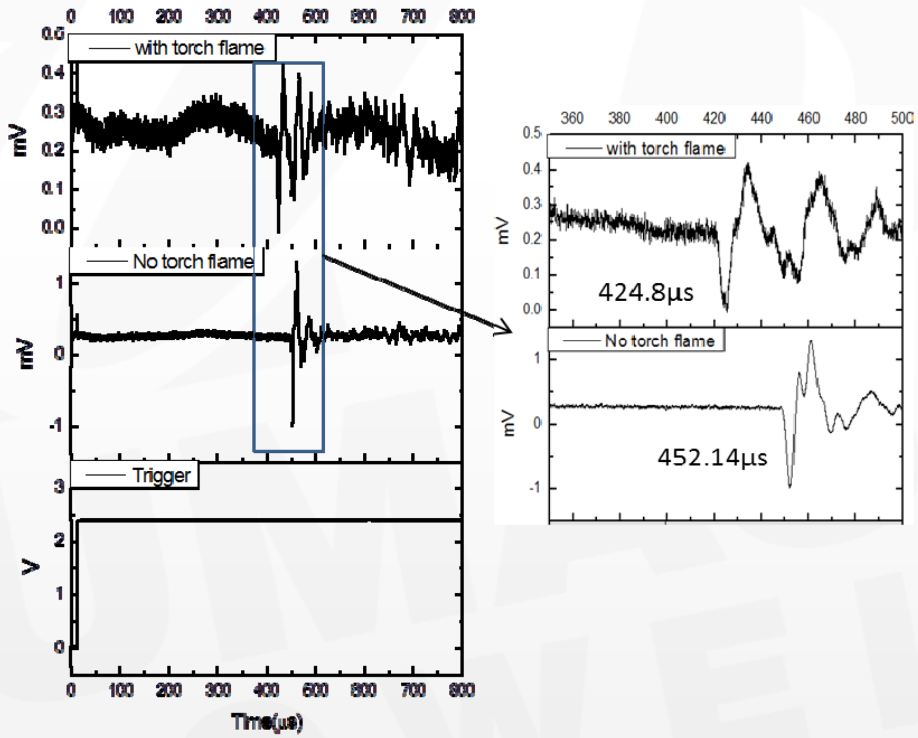

Experimental results of air temperature test in time domain.

- Note: It demonstrated that fiber optic ultrasound transducer system was able to measure the air temperature.

Air temperature reconstruction

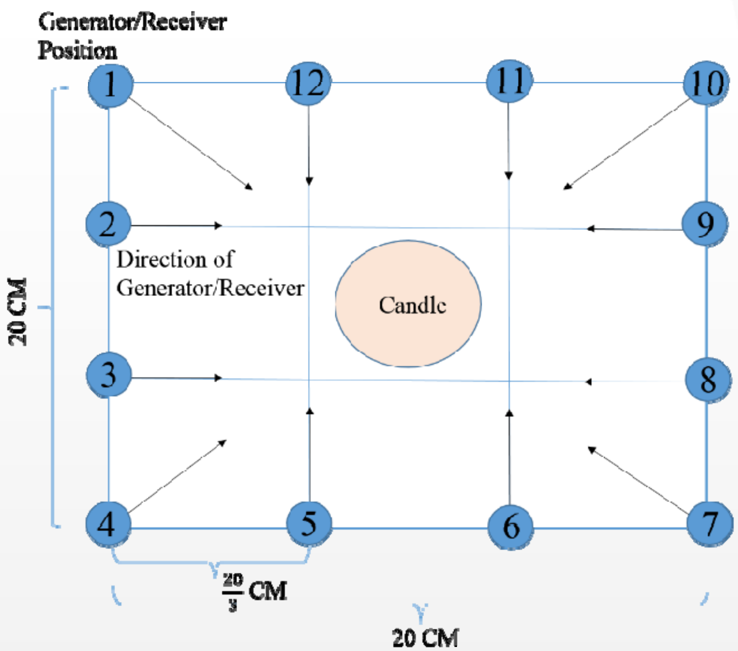

Air temperature test experimental setup [11].
(Top view)

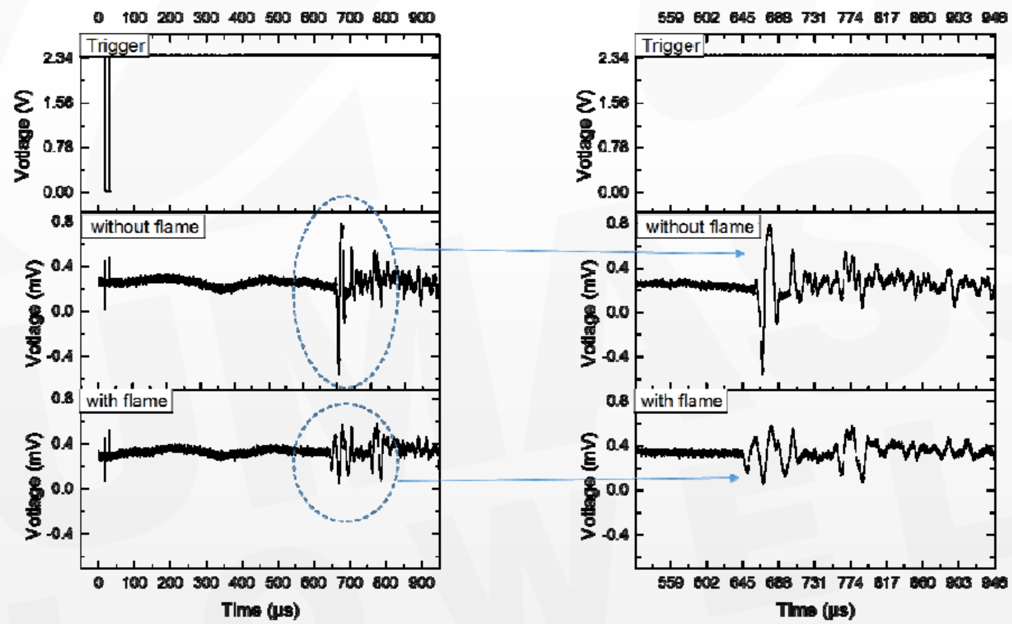

Ultrasound signal between positions 2 and 8

- Note: Air temperature reconstruction was done by using this fiber optic ultrasound transducer system [11].

Distributed sensing capability test

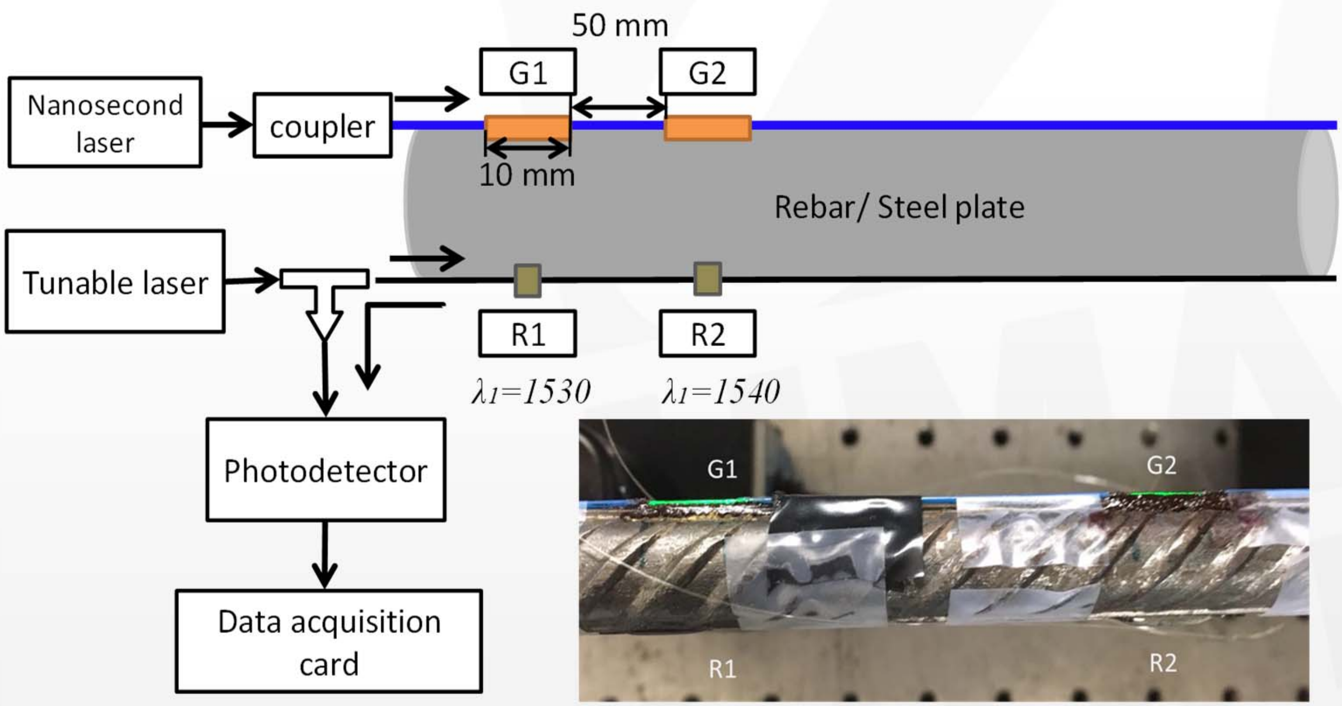

- Sidewall fiber generators (G1 and G2) and the FBG sensors (R1 and R2) were attached on the ridge of the rebar. The FBG sensors were attached along the ridge of rebar using epoxy.

Distributed sensing capability test

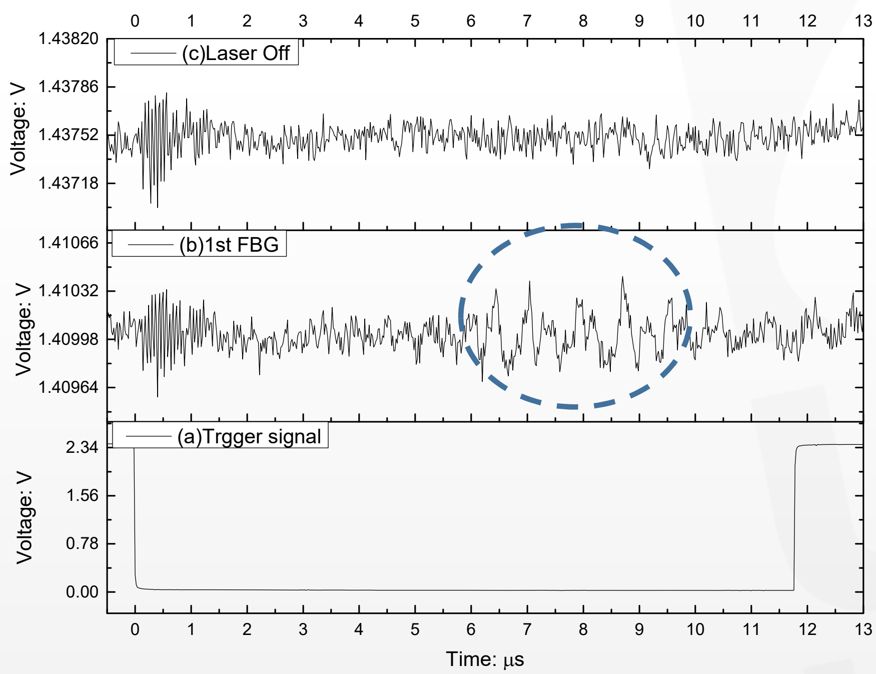

Ultrasound signal detected by R1

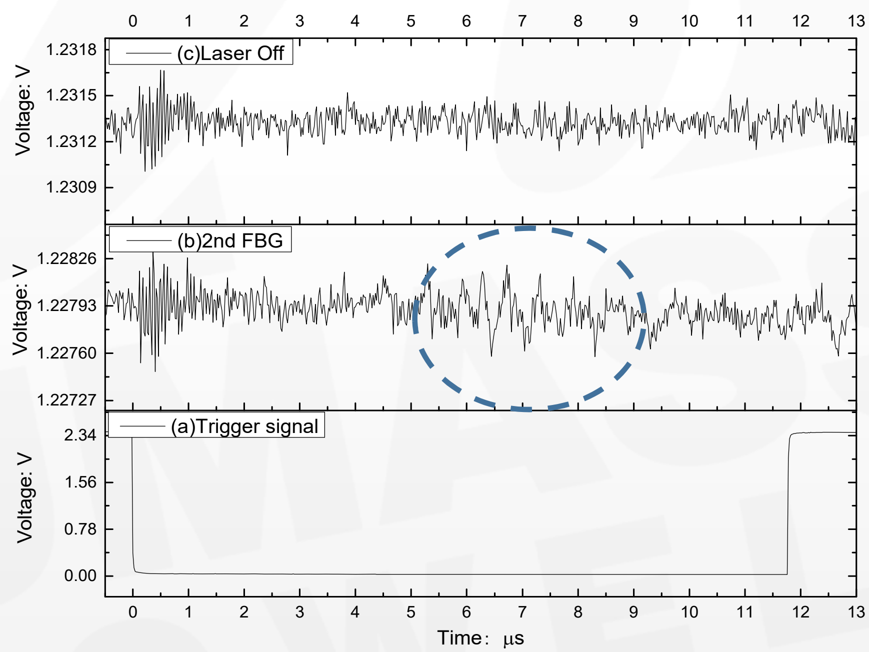

Ultrasound signal detected by R2

- Note: Ultrasound signal was detected in both receivers. This experimental demonstrated that the fiber optic ultrasound transducer system was able to use as multiple points at one time.

GE pilot test

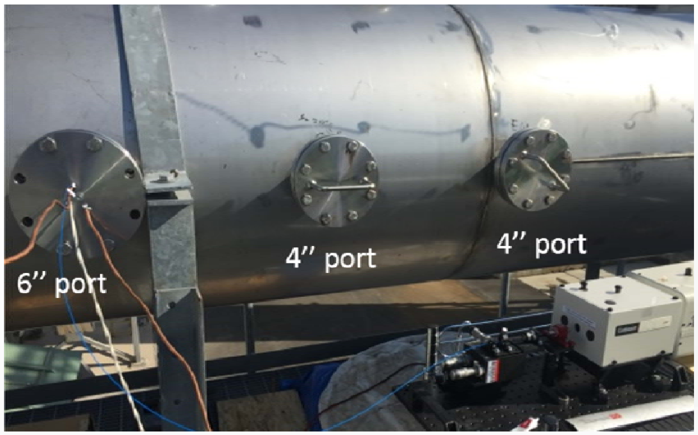

Testing port on exhausting pipe of the ISBF

- Note: The test location was chosen within an exhausting pipe of the ISBF. There are three standard ports along the pipe. The temperature within the pipe is around 480 ° F when the burner starts. Two sensing systems which are based on an electrical method and an optical method, respectively, were used in the pilot test.

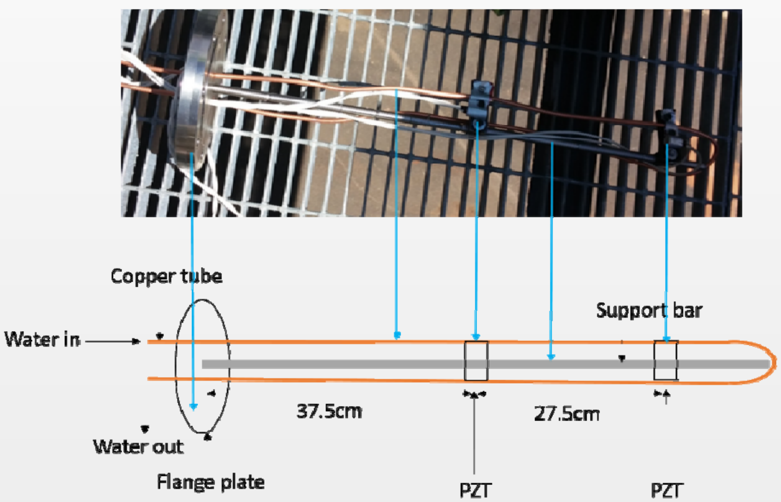

Photo of electrical temperature sensing system

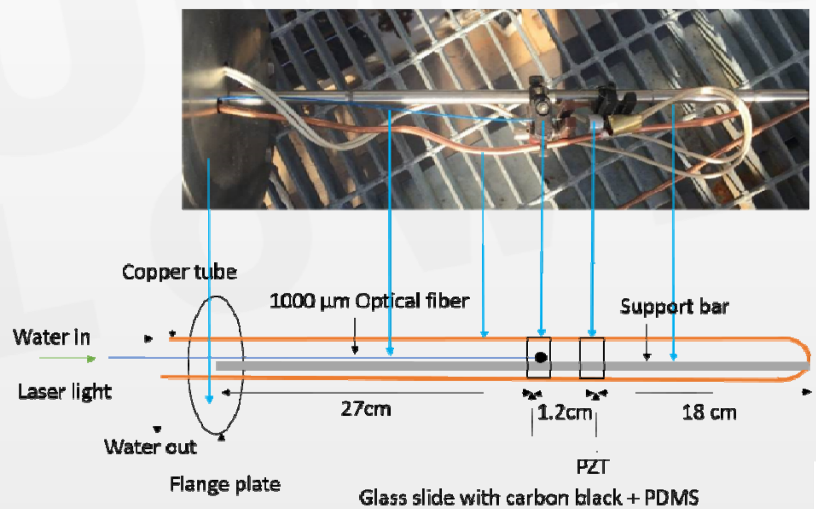

Photo of optical temperature sensing system

GE pilot test

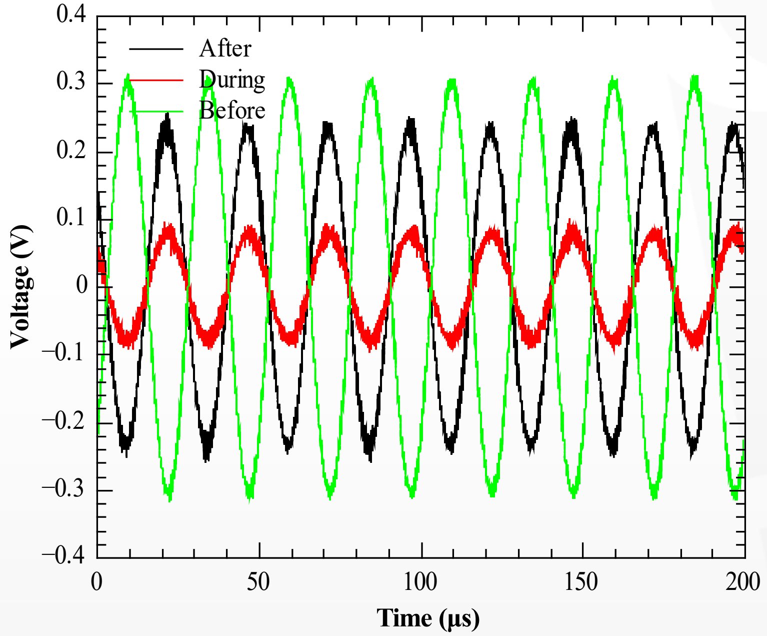

A typical acoustic data obtained from the electrical temperature sensing system.

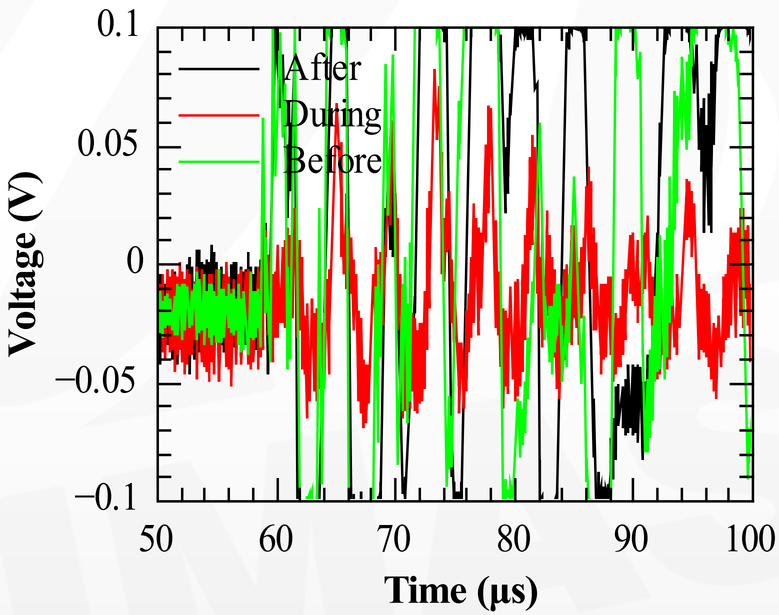

A typical acoustic signal from the optical temperature sensing system.

- Note: Both sensing systems successfully picked up the acoustic signal changes due to the temperature variation. Both sensing systems survived the high temperature environment.
- The optically generated acoustic signal was not strong enough. This also limited the distance between the acoustic emitter and the acoustic receiver.
- More discussion about the GE pilot test is shown on the signal processing part.

Furnace test

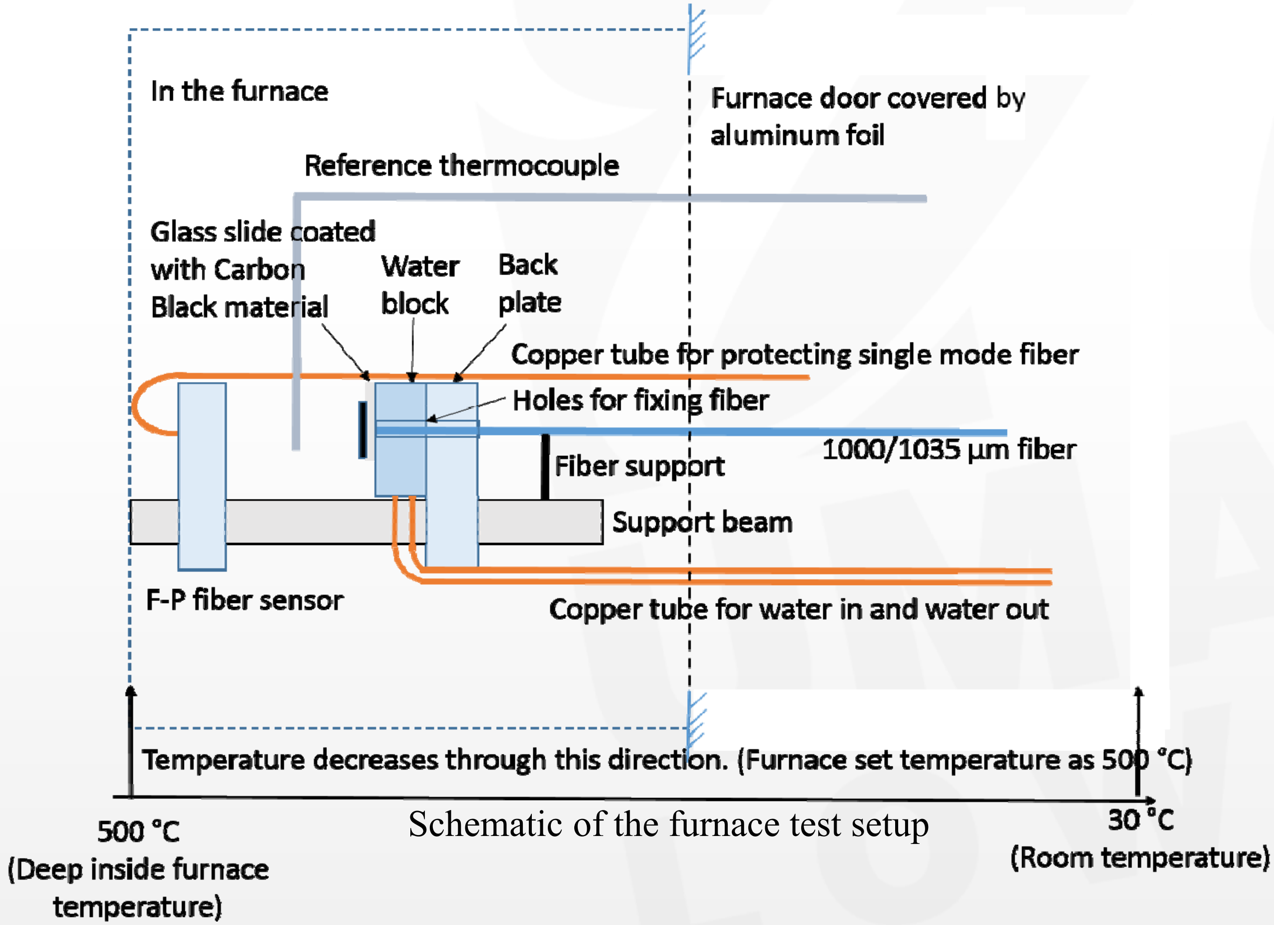

Schematic of the furnace test setup

- Note: The F-P fiber sensor (V20170207TEST1) was used as the signal receiver. The Carbon Black shone by a 1000/1035 μm fiber was used as the acoustic signal generator. The water cooling system was used in this test. The distance between the generator and the receiver was fixed as 10 mm. The furnace temperature was set at room temperature (30 ºC) to high temperature (500 ºC). The furnace door was covered by aluminum foil during the test.

Furnace test

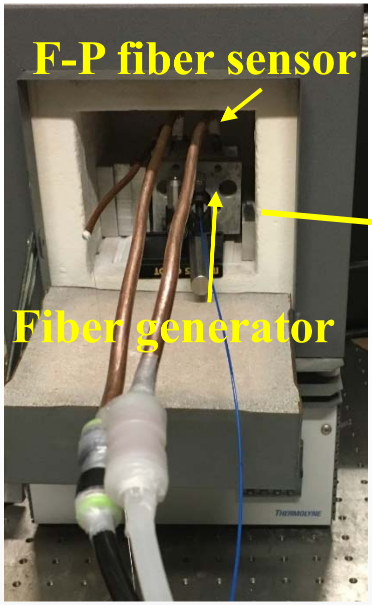

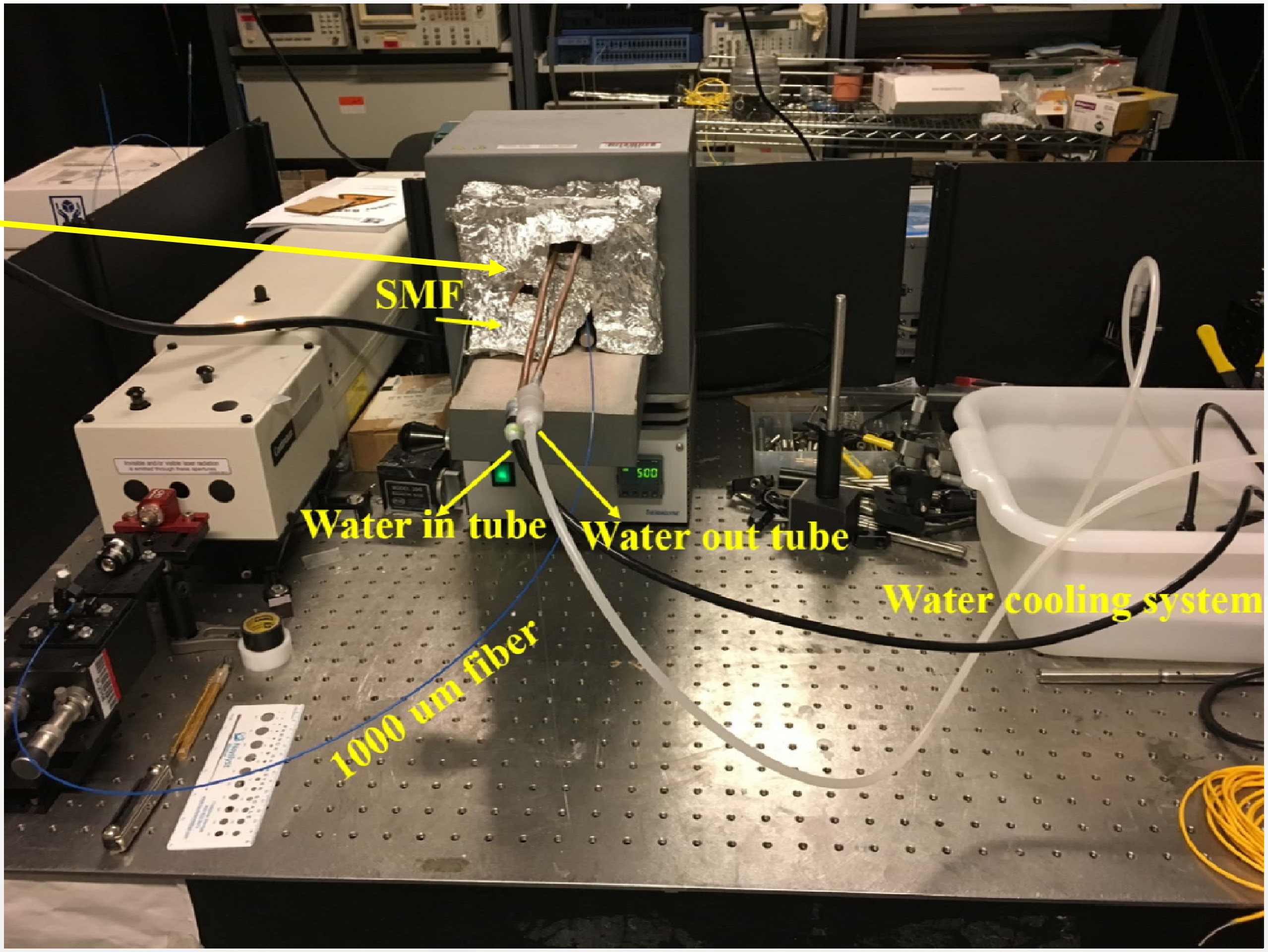

Photo of furnace test setup

Furnace test

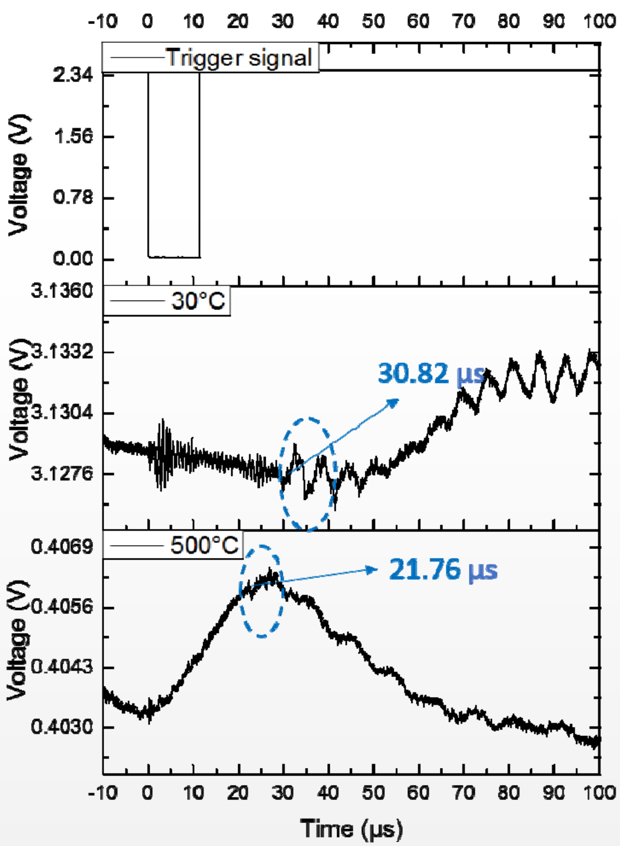

Ultrasound signal when the furnace setting temperature at 30 ºC (room temperature) and 500 ºC.

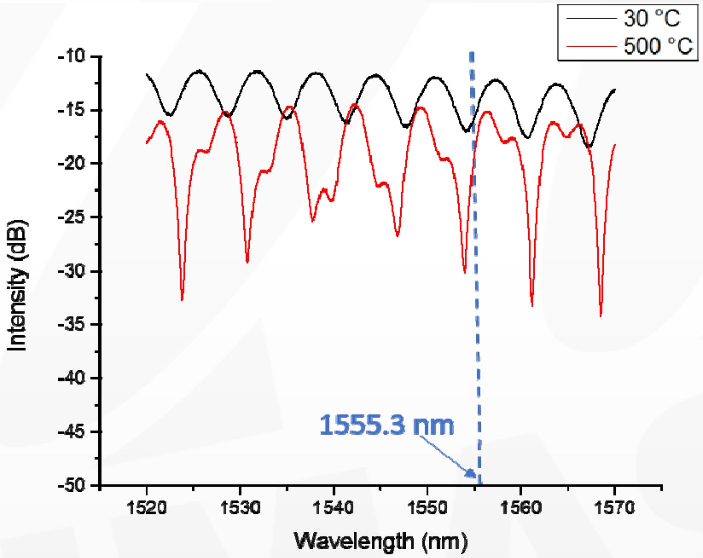

F-P fiber sensor spectrum when the furnace setting temperature at 30 ºC (room temperature) and 500 ºC

- Note: Since we didn't know if the distance between generator and receiver was exactly 10 mm, we used the sound speed at 30 ºC which was 349.02 m/s to calculate the real distance.
- $349.02\ \frac{m}{s} \times 30.82\ \mu s\ =\ 10.76\ \text{mm}$
- $\frac{10.76\ \text{mm}}{21.76\ \mu\text{s}} = 494.49\frac{\text{m}}{\text{s}}$, which represent 334.63 ºC according to the temperature and speed equation; [http://www.sengpielaudio.com/calculator-speedsound.htm]

Furnace test

Furnace setting temperature (ºC)	Temperature reading between the generator and the receiver from a thermocouple (ºC)	Temperature calculated based on the travel time (ºC)
30	30	30
100	49	53.82
300	207	212.2
500	350	334.63

The relationship between the different temperatures .

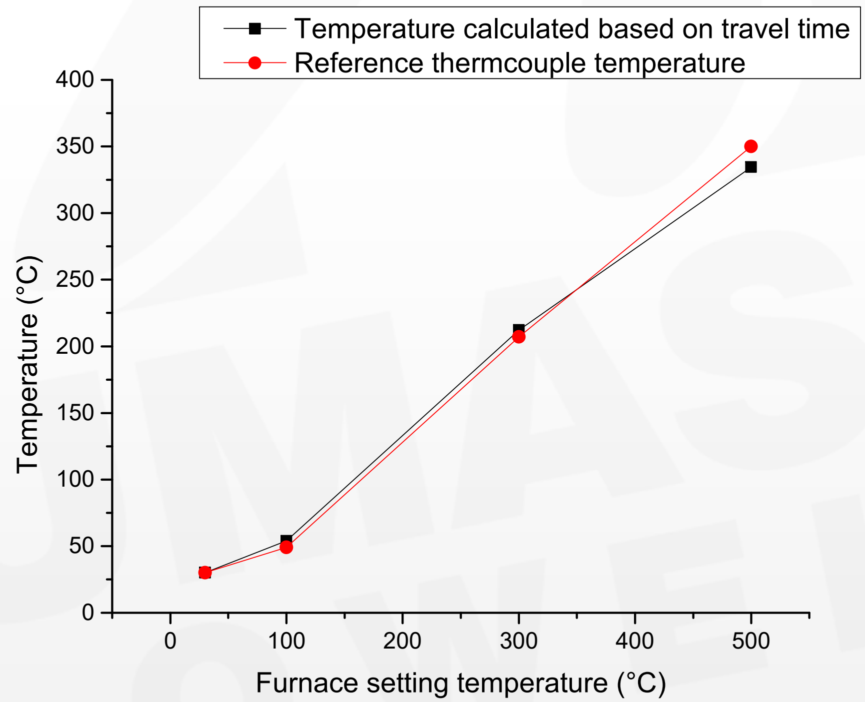

Thermocouple reference temperature compared with temperature calculated based on travel time at the same furnace setting temperature.

Outline

- Brief overview of DOE project
- Sensing system development
- Signal processing and temperature field reconstruction
  1. Signal processing for pulsed acoustic signal
  2. Signal processing for coded sinusoidal acoustic signal
  3. Temperature reconstruction algorithm with GRBF
- Conclusions & Future work

Signal Processing for Pulsed Acoustic Signal

Optically Generated Acoustic Pulse Signal (Pilot Test)

- Acoustic receiver sampling rate: 50MHz
- Emitter: Acoustic optical fiber -- pulse acoustic signal
- Signal detection: sliding correlation

- The ***idea*** of signal processing:

Maximum value of correlation indicates signal arrival.

Signal: Maximum value of correlation (signal & reference coincide in time)
Noise: Value of correlation without signal
SNR: Signal to noise ratio (Signal/Noise)

- The ***procedure*** of signal processing is shown as follow:
  - Filtered signal with band-pass filter : 200kHz – 250kHz
  - Sliding correlation : two methods

Step 1: Band filtering

Using Chebyshev filter with pass-band: 200kHz to 250kHz

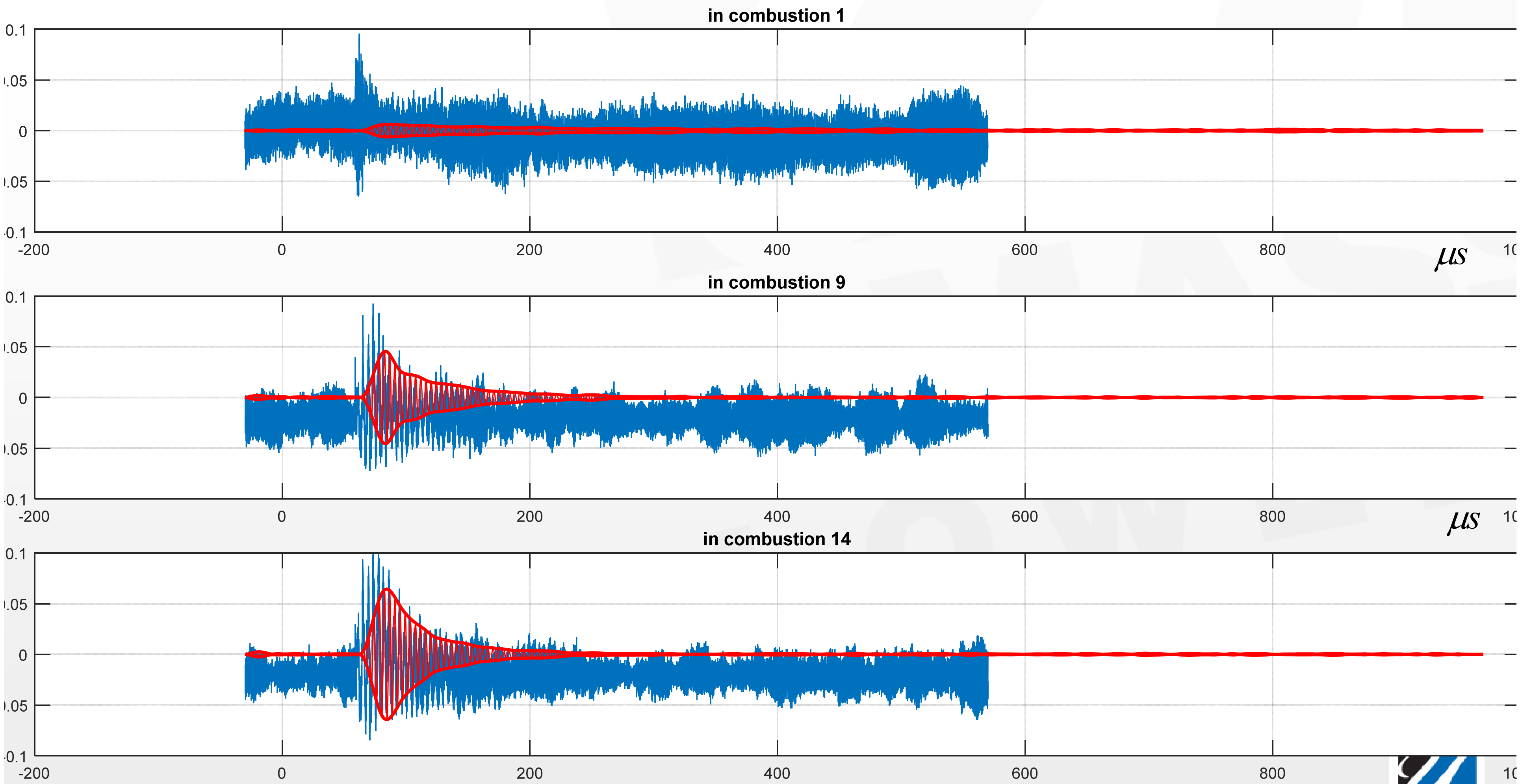

Step 2: Sliding Correlation (Method 1)

- ***Method 1***:
  1. Obtain envelopes of both reference and filtered signals
  2. Calculate correlation of envelopes

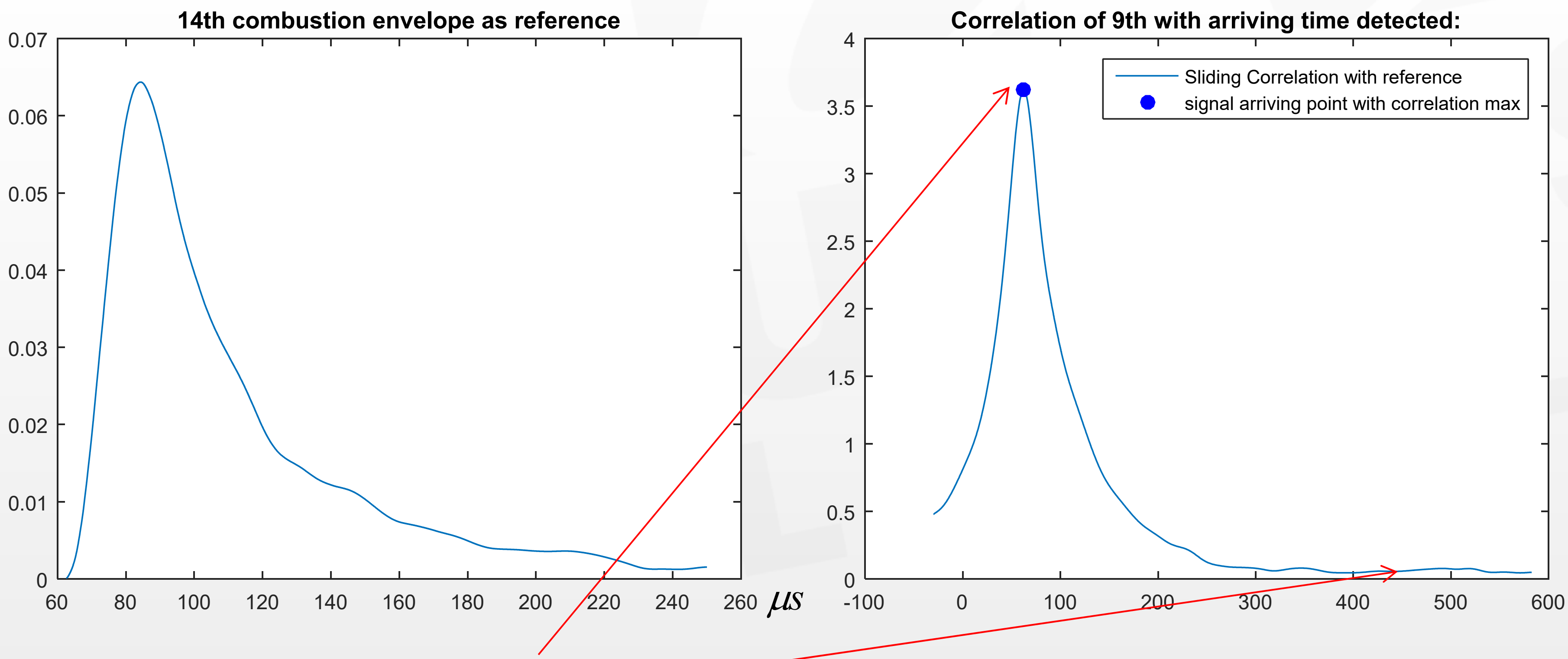

Signal to noise ratio (SNR) > 300

Step 2: Sliding Correlation (Method 2)

- ***Method 2***:
  1. Calculate correlation between filtered signal and reference
  2. Obtain envelope of correlation

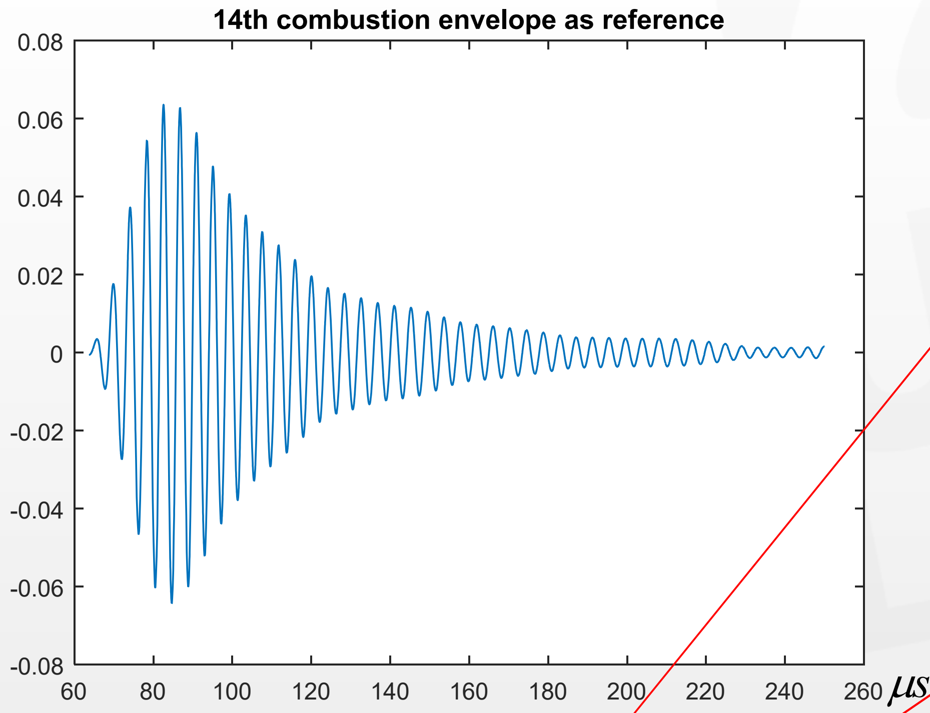

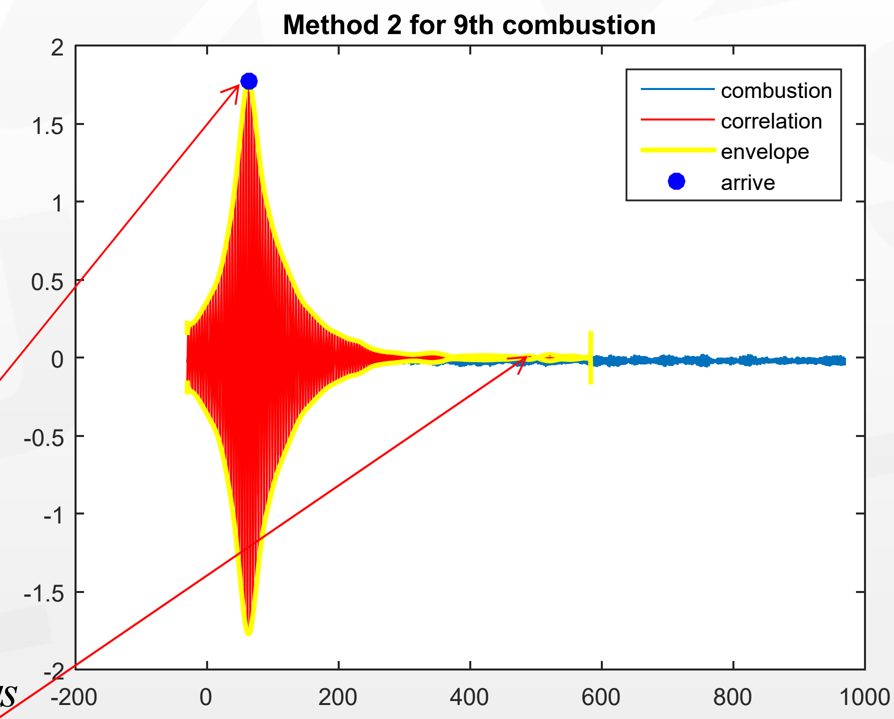

Signal to noise ratio (SNR) > 300

Overall Pilot Test Results

Case	1st method	compare to 14	Relative Arrival Time (us)	2nd method	compare to 14	Relative Arrival Time (us)
Between 1	4415.00	-217.00	-4.34	4402.00	-283.00	-5.66
Combustion 1	4850.00	218.00	4.36	4926.00	241.00	4.82
	4603.00	-29.00	-0.58	4648.00	-37.00	-0.74
	4580.00	-52.00	-1.04	4623.00	-62.00	-1.24
Between 2	4488.00	-144.00	-2.88	4420.00	-265.00	-5.30
Combustion 2	4609.00	-23.00	-0.46	4652.00	-33.00	-0.66
	4589.00	-43.00	-0.86	4634.00	-51.00	-1.02
	4613.00	-19.00	-0.38	4653.00	-32.00	-0.64
Between 3	4493.00	-139.00	-2.78	44.36.00	-249.00	-4.98
Combustion 3	4622.00	-10.00	-0.20	4626.00	-59.00	-1.18
	4598.00	-34.00	-0.68	4646.00	-39.00	-0.78
	4620.00	-12.00	-0.24	4671.00	-14.00	-0.28
Between 4	4630.00	-2.00	-0.04	4565.00	-120.00	-2.40
Combustion 4	4617.00	-15.00	-0.30	4666.00	-19.00	-0.38
	4640.00	8.00	0.16	4689.00	4.00	0.08
	4657.00	25.00	0.50	4690.00	5.00	0.10
Combustion 5	4611.00	-21.00	-0.42	4656.00	-29.00	-0.58
	4632.00 (*refer*)	0.00	0.00	4685.00	0.00	0.00
	4630.00	-2.00	-0.04	4677.00	-8.00	-0.16
Between 5	4520.00	-112.00	-2.24	4467.00	-218.00	-4.36
Combustion 6	4523.00	-109.00	-2.18	4481.00	-204.00	-4.08
	4593.00	-39.00	-0.78	4644.00	-41.00	-0.82
	4623.00	-9.00	-0.18	4676.00	-9.00	-0.18

Overal Pilot Tests Results

Arriving Time Interval in combustion using different method

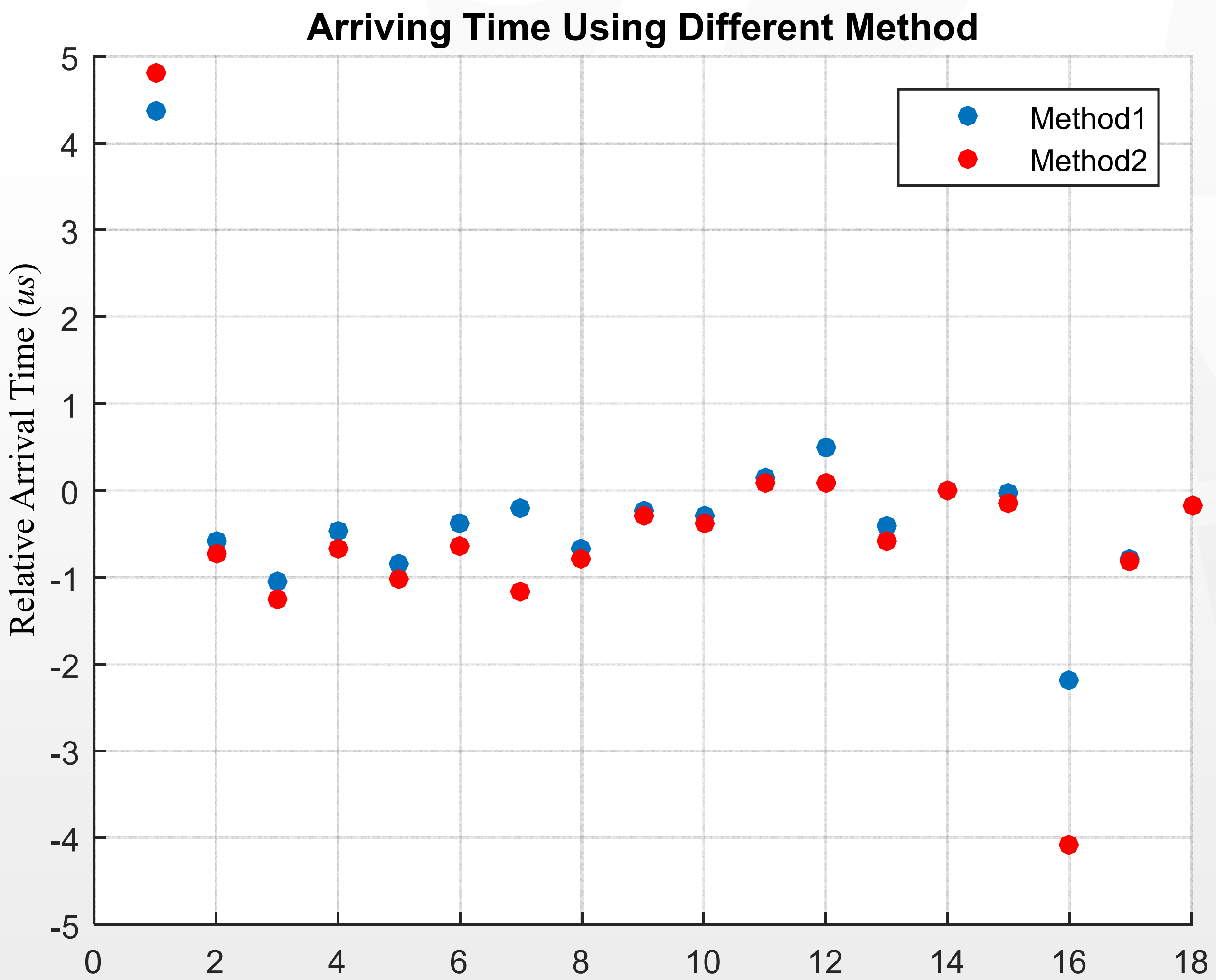

Signal Processing for Coded Sinusoidal Signals

Case 2 : Code Division Multiple Access (CDMA) Scheme

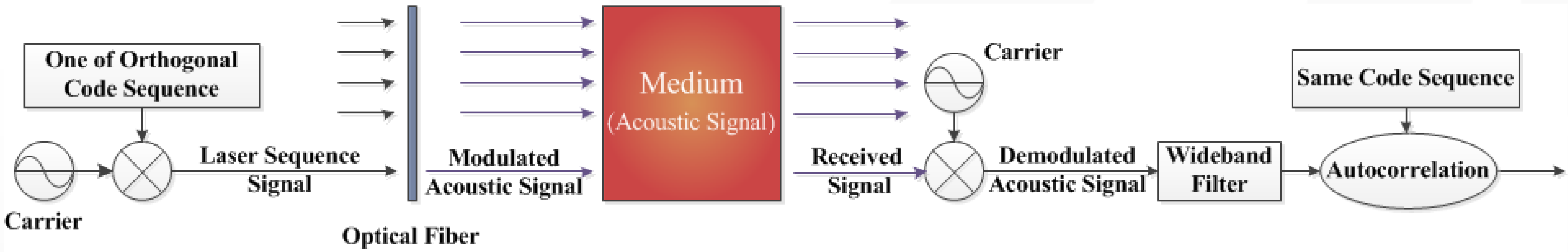

- ❑ Orthogonal Code based coding:
  - Enable parallel multiplexing mode
    - ✓ Multi-channel
  - Increase Signal to Noise Ratio (SNR)

Method:

Assign each emitters with a code from a set of orthogonal pseudo-random sequences

Design Parameters

- Design Parameters

  - f : the acoustic carrier signal frequency (fixed during the test)
  - L: Number of bits in the code
  - M: cycles of carrier signal for one bit of code

- Performance
  - Number of channels: L
  - Time-of-flight (TOF) sampling rate: $\frac{f}{LM}$
  - SNR and uncertainty : Proportional to LM

Analysis for SNR and Uncertainty

- The signal captured by the *i-th* receiver at time index

$$I_i(m,n,k) = S_0(m,n,k) + D(m,n,\alpha,\beta)P_i(k)$$

$D(m,n,\alpha,\beta)P_i(k)$	acoustic signal with its magnitude $P_i(k)$ coded as pseudorandom sequences
$S_0(m,n,k)$	noise and other transmitters' signal
m,n	spatial distribution of the acoustic signal

- Correlation and autocorrelation
  - Correlation of the received signal with the original acoustic signal:

$$R_i(k) = \sum_{k-N}^{k} I(m,n,k)P_i(k),$$

where $N = L * M$, is the length of signal $P(k)$.

  - Correlation of the noise signal with original acoustic signal:

Assume the distribution of $S_0(m,n)$ is at mean *0*, with variance σ^2

$$R_0(k) = \sum_{k-N}^{k} S_0(m,n,k)P_i(k),$$

$$var[R_0(k)] = \frac{\sigma^2}{N}\sum_{k-N}^{k} P_i(k) = \sigma_n^2.$$

If S_0 and P_i are irrelevant, $R_0(k)$ would be very close to 0.

SNR Simulation Results

- **SNR testing results for different length (fixed f and M)**

  -- add Gaussian white noise as back ground noise

$$SNR(dB) = 10log_{10}\left(\frac{P_{signal}}{P_{noise}}\right) = 20log_{10}\left(\frac{A_{signal}}{A_{noise}}\right).$$

Order n	L $(2^n - 1)$	SNR (dB)
5	31	-10
6	63	-20
7	127	-25
8	255	-30
9	511	-35
10	1023	-40
11	2047	-45

Pilot Test Setup

- Pilot test setup:
- Emitter: PZT -- sinusoidal acoustic signal (from ***pilot test*** measurement)

  activate emitter *twice*:

  at t = 8ms & at t = 16ms.
- Frequency of PZT : f=400kHz
- Sampling rate : 50MHz

- Signal coding is simulated using segments of experimental data
  - L=31 bits per code
  - M=100 cycles per bit
  - Allows 31 channels simulataneously
  - ToF sampling rate = 129 Hz
  - SNR (simulated in following slides)

SNR

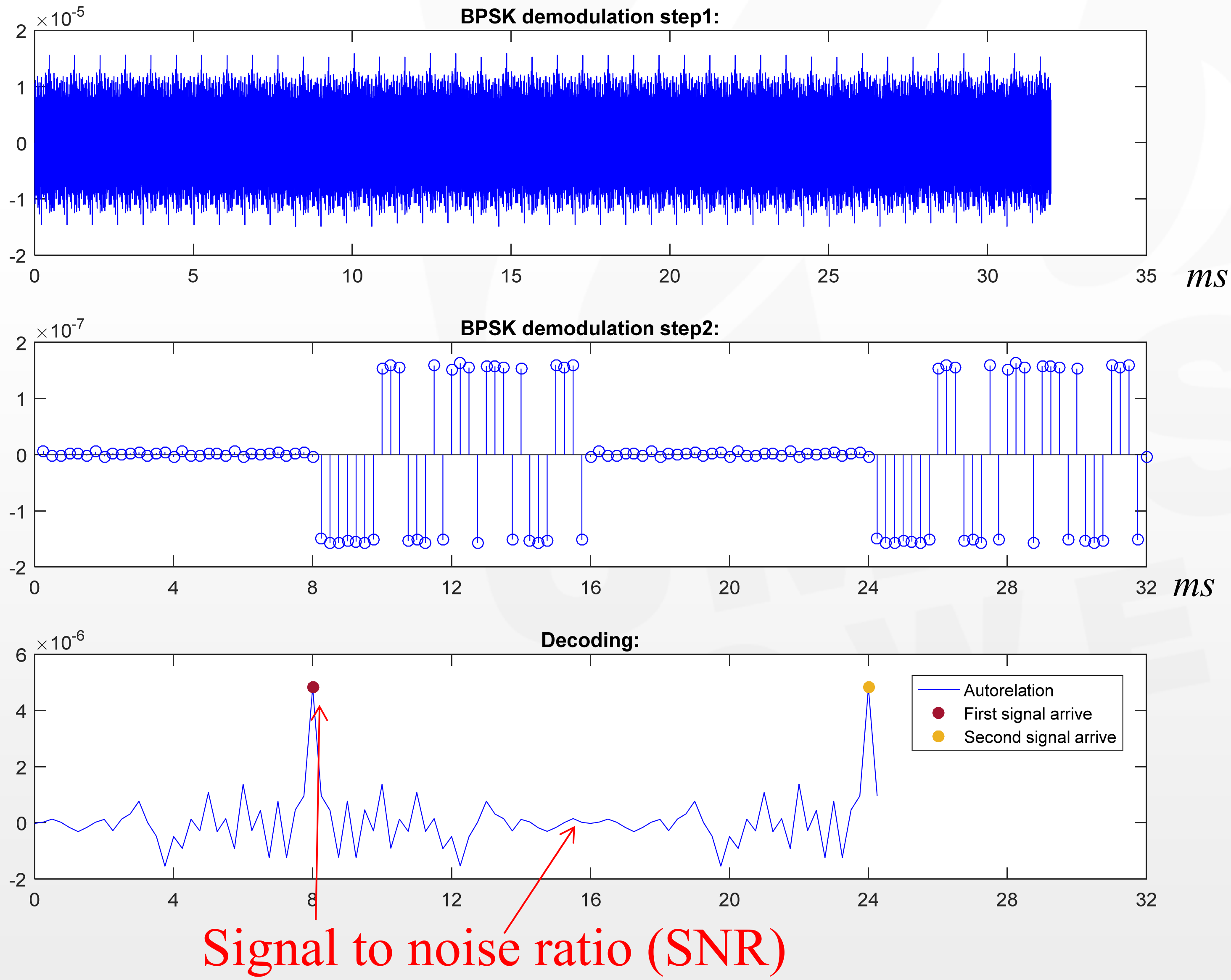

BPSK demodulation step1:
×10^-5
ms
BPSK demodulation step2:
×10^-7
ms
Decoding:
×10^-6
Autorelation
First signal arrive
Second signal arrive
Signal to noise ratio (SNR)

SNR - Continued

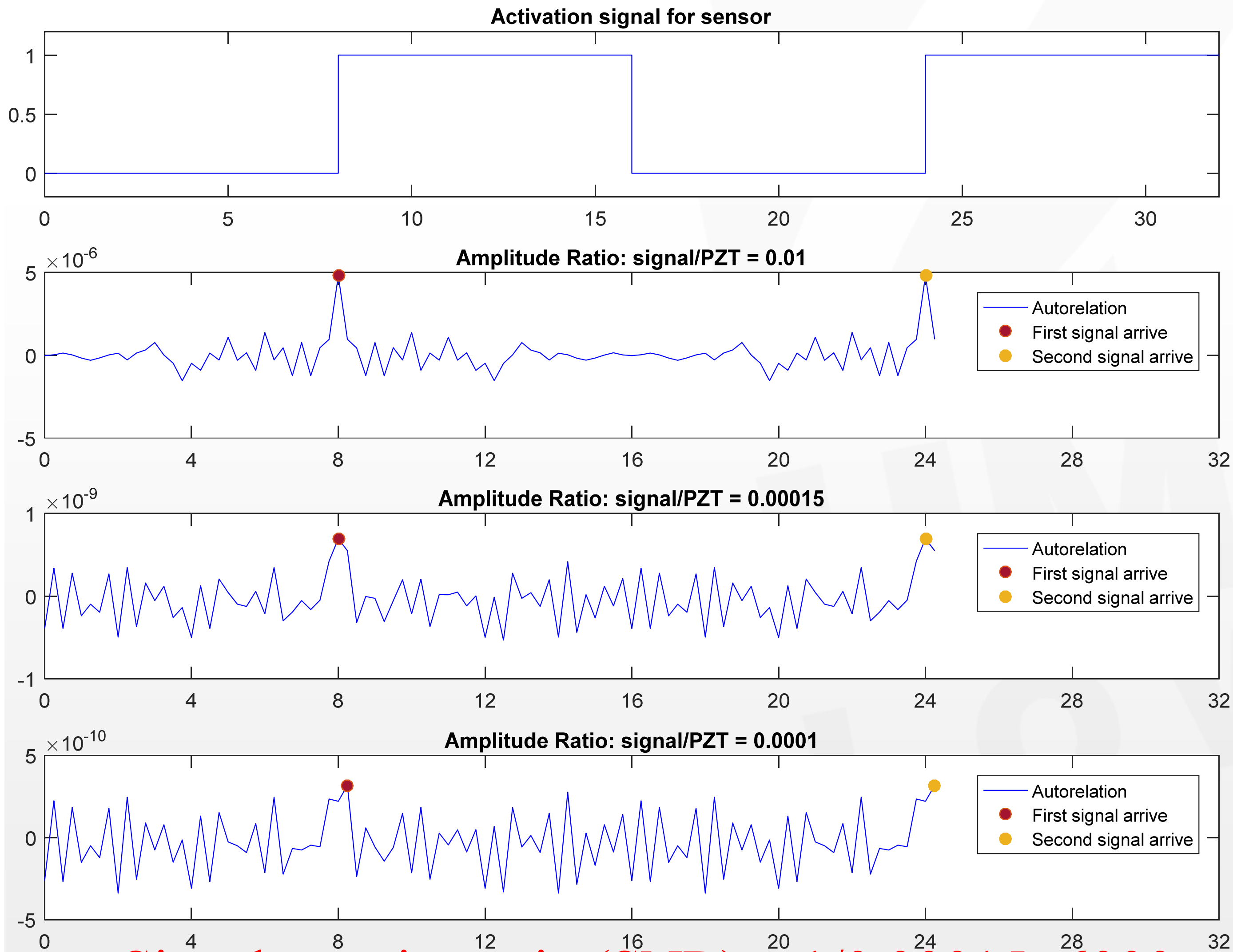

Same noise

Multiply signal by

0.01

0.00015 (still work)

0.0001 (starting to fail)

Signal to noise ratio (SNR) ≈ 1/0.00015>6000

On-going work: Uncertainty Analysis

Correlation of the original acoustic signal

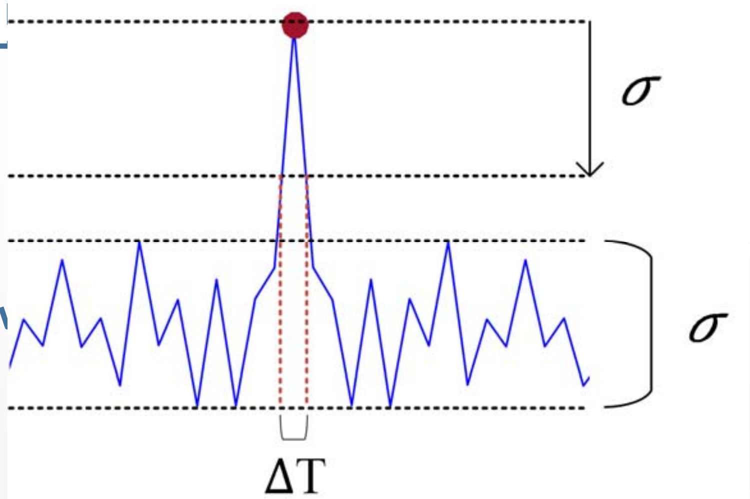

ΔT is the uncertainty for TOF measurement.

Signal Processing: Results

Considering a simplified free field that acoustic attenuation is only due to scattering.
A doubling of the distance from a noise source reduces the sound pressure with 6dB.

	Optically driven pulse signal	PCT code modulated sin wave
SNR (20cm distance)	300 (24.7dB)	6000 (378dB)
Signal duration	0.2ms (receiver side)	7.8ms
Correlation signal width	≈0.3ms (Better for uncertainties)	≈2.5ms
Expected distance that ToF can still be picked up*	3m	15m

*Using same emitter and receiver setup as in pilot tests

Overall efficiency similar

Temperature Field Reconstruction Algorithm

- ❑ polynomial interpolation approximation and Taylor expansion
  - ✓ a finite summation of polynomial series with residual error
  - ✓ a global method, for function with local property, it cannot demonstrate good accuracy

- ❑ Fourier parameterization
  - ✓a summation of simple oscillating functions (sines and cosines)
  - ✓Gibbs Phenomenon: large oscillations near the jump discontinuity
  - ✓cannot be applied to complex geometries

- ❑ GRBF
  - ✓ better approximation capabilities for most nonlinear functions
  - ✓ superior in scalability
  - ✓ more efficient for higher dimensional space and complex geometry
  - ✓ exponentially convergent
  - ✓ good local property

Temperature Field Reconstruction Algorithm with GRBF

- GRBF

$$\phi_i(\mathrm{X}) = e^{-\frac{\|X - X_i\|^2}{2\sigma_j^2}}$$

✓ X_i and σ_j are the predefined center and variance, X is position with 3 dimensions

✓ Any continuous nonlinear function can be approximated by the summation of basis functions with appropriate weights

$$f(\mathrm{X}) \approx \sum_{i=1}^{N} \omega_i \phi_i(\mathrm{X})$$

- The relationship between speed of acoustic waves and temperature is as following:

$$v = z\sqrt{T(x,y,z)}$$

- we can approximate the temperature field via GRBF:

$$(z\sqrt{T(x,y,z)})^{-1} = \frac{l_k}{t_k} = \sum_{i=1}^{M} \omega_i \Phi_i(x,y,z) = \sum_{i=1}^{M} \omega_i \exp\{-[(x-X_i)^2 + (y-Y_i)^2 + (z-Z_i)^2]/2\tau^2\}$$

$$= \sum_{i=1}^{M} \omega_i \exp(-\frac{p^2_{ik}}{2\tau^2})$$

p_{ik} is the distance from center of the i_{th} basis function to the k_{th} path

Design Parameter

N: The number of basis functions

Simulation results for different choice of N

N	5	6	7	8	9	10	11
Average absolute error	81.31°C	28.57°C	27.63°C	27.14°C	25.28°C	26.60°C	23.58°C
Average relative error	6.94%	2.53%	2.46%	2.21%	2.19%	2.18%	1.98%

- ❑ Larger N leads to smaller error
- ❑ Benefits decreases as N is large

Simulation Results with GRBF

- 2D temperature field case I:

Unimodal symmetric $T(x,y) = 1000 + 600\sin(\pi x/length)\sin(\pi y/height)$

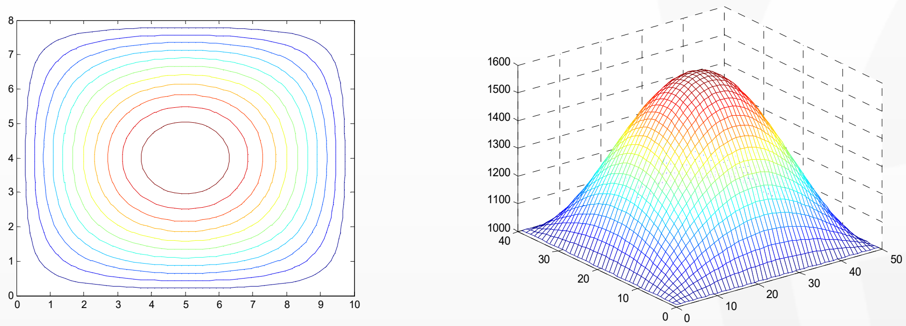

Real Temperature Field

Notes: In the simulation 10 sensors were evenly distributed, 10 basis functions were used, and 24 paths were chosen.

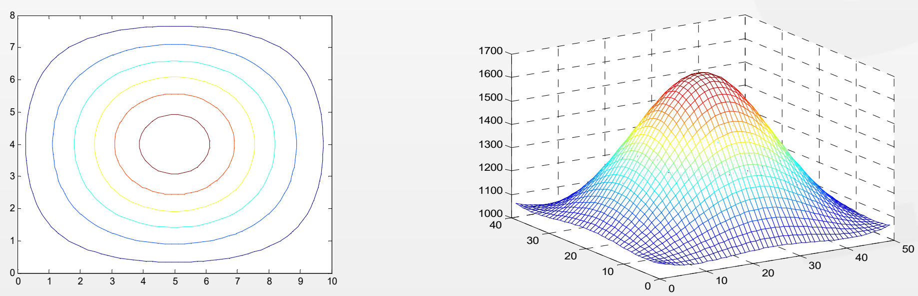

Reconstructed Temperature Field

Simulation Results with GRBF

- 2D temperature field case II:

Unimodal deflection

$$T(x, y) = 600\exp((-(x-4)^2)/length - ((y-3)^2)/(2*height)) + 1000$$

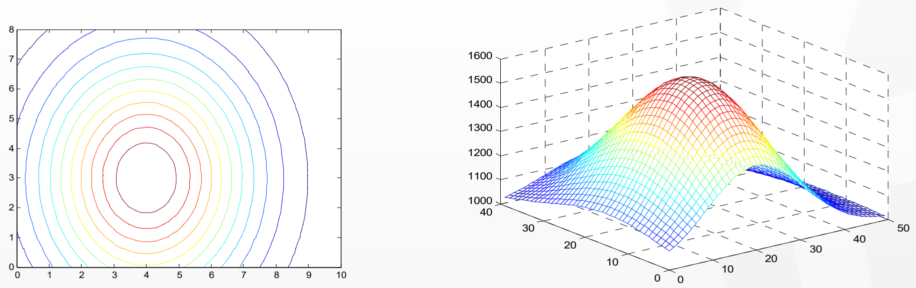

Real Temperature Field

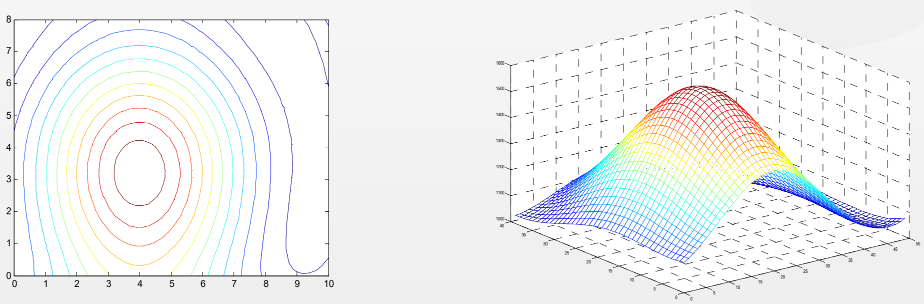

Reconstructed Temperature Field

Notes: In the simulation 10 sensors were evenly distributed, 10 basis functions were used, and 24 paths were chosen.

Simulation Results

Reconstruction Error

Model	Maximum absolute error	Maximum relative error	Average absolute error	Average relative error
Unimodal symmetric	64.6003°C	4.97%	23.5141°C	2.68%
Unimodal deflection	89.8020°C	8.95%	24.9697°C	2.19%

Initial Uncertainty Analysis

Suppose N is the number of basis functions, and M is the number of paths.

Without measurement noise, we have $$\int \sum_{i=1}^{N} \omega_i \phi_i(x,y,z) dl_j = t_j \qquad (i=1,\ldots,N; j=1,\ldots,M)$$

which can be written as

$$\begin{bmatrix} \int \phi_1(x,y,z)dl_1 & \ldots & \int \phi_i(x,y,z)dl_1 & \ldots & \int \phi_N(x,y,z)dl_1 \\ \vdots & \vdots & \vdots & \vdots & \vdots \\ \int \phi_1(x,y,z)dl_j & \cdots & \int \phi_i(x,y,z)dl_j & \cdots & \int \phi_N(x,y,z)dl_j \\ \vdots & \vdots & \vdots & \vdots & \vdots \\ \int \phi_1(x,y,z)dl_M & \cdots & \int \phi_i(x,y,z)dl_M & \cdots & \int \phi_N(x,y,z)dl_M \end{bmatrix} \begin{bmatrix} \omega_1 \\ \vdots \\ \omega_i \\ \vdots \\ \omega_N \end{bmatrix} = \begin{bmatrix} t_1 \\ \vdots \\ t_j \\ \vdots \\ t_M \end{bmatrix}$$

With measurement noise, we have $$\int \sum_{i=1}^{N} \bar{\omega}_i \phi_i(x,y,z) dl_j = t_j + \Delta t_j \qquad (i=1,\ldots,N; j=1,\ldots,M)$$

which can be written as

$$\begin{bmatrix} \int \phi_1(x,y,z)dl_1 & \ldots & \int \phi_i(x,y,z)dl_1 & \ldots & \int \phi_N(x,y,z)dl_1 \\ \vdots & \vdots & \vdots & \vdots & \vdots \\ \int \phi_1(x,y,z)dl_j & \cdots & \int \phi_i(x,y,z)dl_j & \cdots & \int \phi_N(x,y,z)dl_j \\ \vdots & \vdots & \vdots & \vdots & \vdots \\ \int \phi_1(x,y,z)dl_M & \cdots & \int \phi_i(x,y,z)dl_M & \cdots & \int \phi_N(x,y,z)dl_M \end{bmatrix} \begin{bmatrix} \bar{\omega}_1 \\ \vdots \\ \bar{\omega}_i \\ \vdots \\ \bar{\omega}_N \end{bmatrix} = \begin{bmatrix} t_1 + \Delta t_1 \\ \vdots \\ t_j + \Delta t_j \\ \vdots \\ t_M + \Delta t_M \end{bmatrix}$$

Note: Measurement noise in traveling time will propagate into the integral process for reconstruction

Measurement Noise in Travelling Time-Simulation Analysis

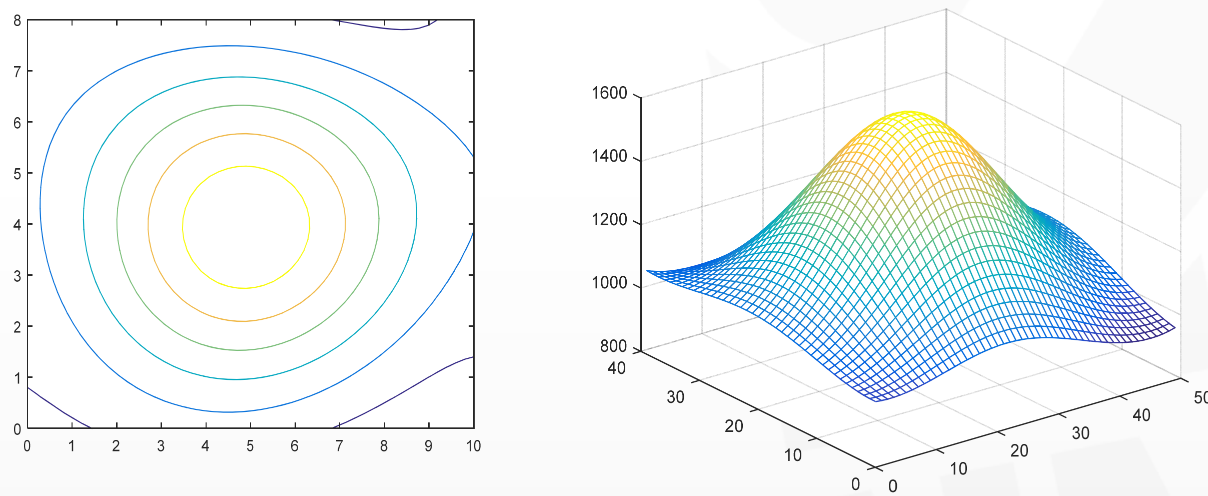

Fig.1. Reconstruction with measurement noise

Measurement noise [Add 1% error in ToF] will propagate into the integral process for reconstruction

1. The maximum absolute error is 91.98 °C
2. The average absolute error is 17.23 °C
3. The maximum relative error is 8.82%
4. The average relative error is 1.47%

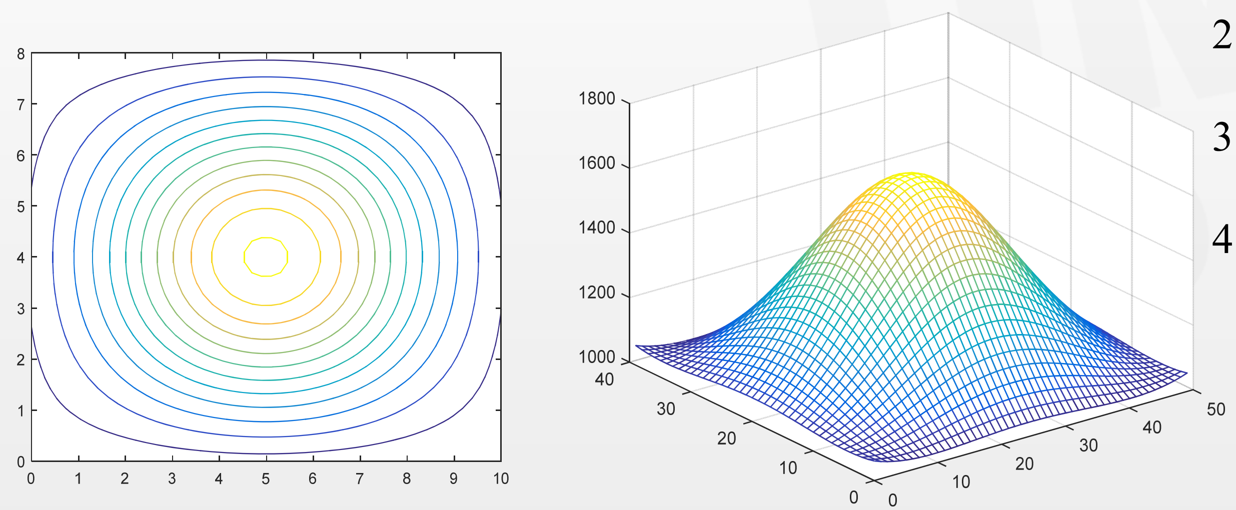

Fig.2. Reconstruction without measurement noise

Experimental Results (candle)

- Sensor location: sensors are distributed symmetrically (**Fig.1**)
- Reconstruction results of temperature field in 2D (**Fig.2**)

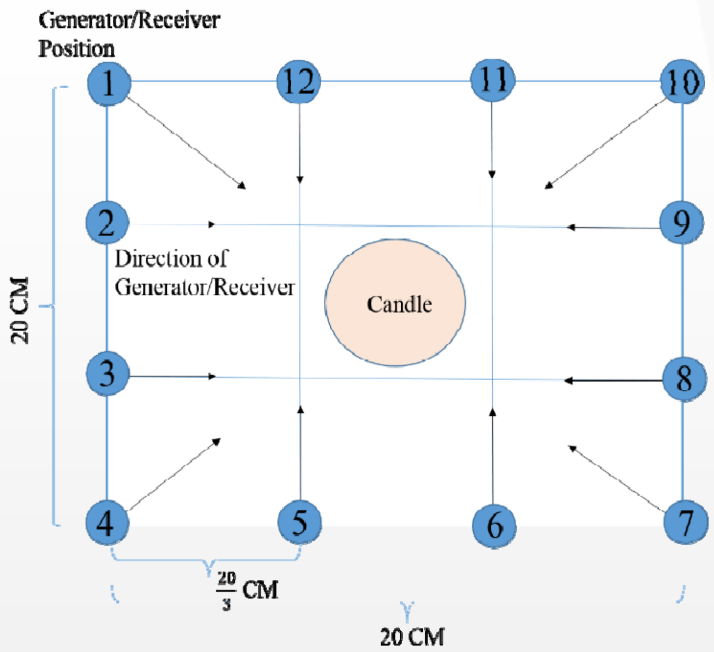

Fig.1. Sensor distribution

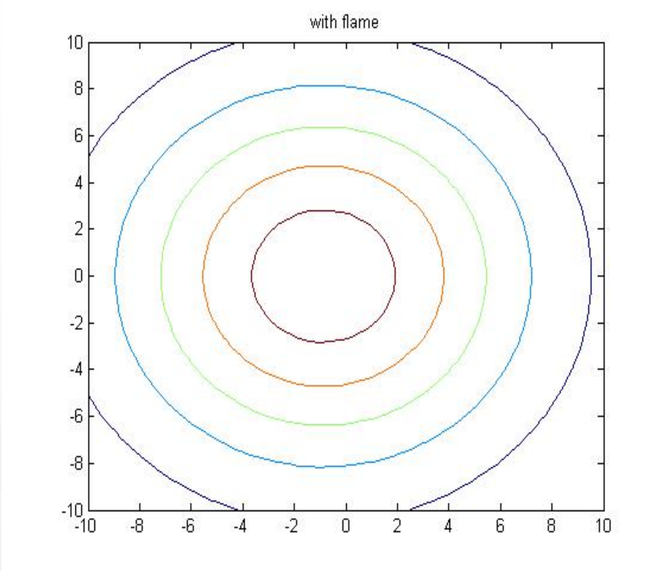

Fig.2. Temperature field

Future Work for Temperature Field Reconstruction

- Assumes no knowledge about the dynamics of temperature field
- A dynamic model of the temperature field exists

❑ Key idea

❖ Utilize known dynamic model of the temperature field

❖ What to be estimated are high dimensional states of the dynamic model

❖ Measurements can be utilized to update states of the temperature field recursively (Kalman Filter).

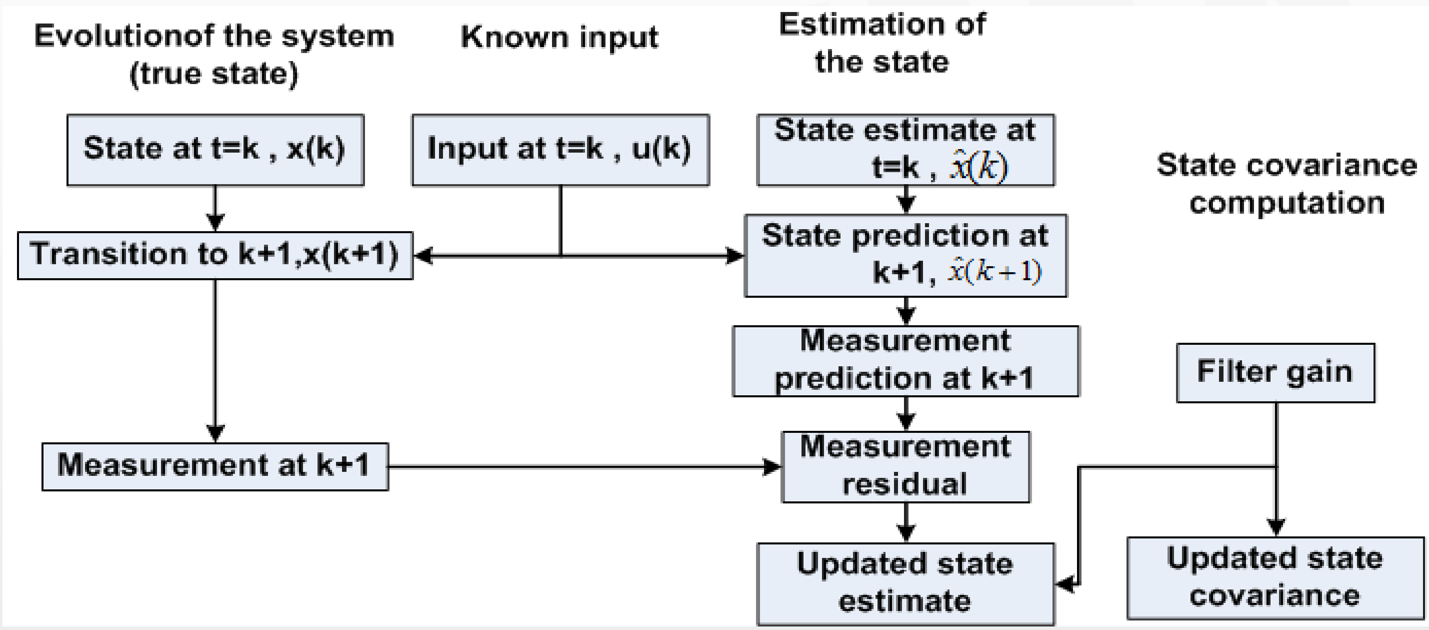

Outline

- ❑ Brief overview of DOE project
- ❑ Sensing system development
- ❑ Signal processing and temperature field reconstruction
- ❑ Conclusions & Future work

Conclusions

➢ What we have achieved.

1. Temperature test in water condition has been conducted.
2. Temperature test in a steel plate has been conducted.
3. Temperature test in air condition (furnace) has been conducted.

The temperature range for our all-optical fiber system in air condition (furnace) was 19 ºC - 500 ºC.

4. The pilot test conducted in GE has proved our system is workable.
5. ToF can be detected with high SNR in pilot tests.
6. Optically driven acoustic emitter is comparable in efficiency to PCT transducer used .
7. Based on the pilot test results, it is optimistic that the sensors and signal processing will work in the scale of meters.

7. This Project has partially supported 1 postdoctoral researcher, 3 PhD students, 1 master student and 2 undergraduate students.

8. Five conference papers have been published. Three journal papers are in preparation.

Acknowledgement

1. We would like to thank the Department of Energy and our project manager, Jessica Mullen, for sponsoring this work (FE0023031).
2. We would like to thank Dr. Xinsheng Lou and Mr. Carl Edberg at General Electric for supporting the pilot test.
3. We would like to thank Mr. Junwei Su for assisting in machining the packaging system.

Publications and Reference

- [1] Jingcheng Zhou, Nan Wu, Xingwei Wang, Yuqian Liu, Tong Ma, Daniel Coxe, Chengyu Cao, “Water temperature measurement using a novel fiber optic ultrasound transducer system”, IEEE International Conference on Information and Automation, Lijiang, China, August 8-10, 2015
- [2] Xiaotian Zou, Nan Wu, Ye Tian, and Xingwei Wang, "Broadband miniature fiber optic ultrasound generator", Virtual Journal for Biomedical Optics, 9(9), 18119, 2014
- [3] Ye Tian, Nan Wu, Kai Sun, Xiaotian Zou, and Xingwei Wang, “Numerical simulation of fiber-optic photoacoustic generator using nanocomposite materials”, Journal of Computational Acoustics, 21(2), 1350002, 2013
- [4] Jingcheng Zhou, Nan Wu, Siwen Bi and Xingwei Wang, ”Ultrasound generation from an optical fiber sidewall” SPIE Smart Structures/NDE 2016
- [5] Siwen Bi, Nan Wu, Jingcheng Zhou, Xingwei Wang, Tong Ma, Yuqian Liu and Chengyu Cao, “Ultrasonic temperature measurements with fiber optic system” SPIE Smart Structures/NDE 2016
- [6] Nan Wu, Xiaotian Zou, Jingcheng Zhou and Xingwei Wang, "Fiber optic ultrasound transmitters and their applications", Measurement, Volume 79, 164-171, 2016
- [7] Nan Wu, Ye Tian, Xiaotian Zou, Vinicius Silva, Armand Chery, and Xingwei Wang, "High-efficiency optical ultrasound generation using one-pot synthesized polydimethylsiloxane-gold nanoparticle nanocomposite", Journal of the Optical Society of America B, 29(8), 2016-2020 2012
- [8] Ye Tian, Nan Wu, Kai Sun, Xiaotian Zou, and Xingwei Wang, “Numerical simulation of fiber-optic photoacoustic generator using nanocomposite materials”, Journal of Computational Acoustics, 21(2), 1350002, 2013
- [9] Xiaotian Zou, Nan Wu, Ye Tian, Yang Zhang and Xingwei Wang, "Polydimethylsiloxane thin film characterization using all-optical photoacoustic mechanism", Applied Optics, 52(25), 6239-6244, 2013
- [10] Xiaotian Zou, Tyler Schmitt, David Perloff, Nan Wu, Tzu-Yang Yu, and Xingwei Wang, "Nondestructive corrosion detection using fiber optic photoacoustic ultrasound generator", Measurement, Volume 62, 74-80, 2014
- [11] Jingcheng Zhou, Nan Wu, Tong Ma, Xu Guo, Cong Du, Yuqian Liu, Chengyu Cao and Xingwei Wang, "Proof of concept temperature field monitoring using optically generated acoustic waves sensing", 59th ISA POWID Symposium, Charlotte, North Carolina USA, June 27-30, 2016.

Patent

Patent:

- 2016 Xingwei Wang, Nan Wu, “Photoacoustic Probe”, WO2016178981 A1, WO2012112890A2; EP2675361A2; US20130319123A1; WO2012112890A3.
- PCT nationalization coming up in November.
- Academic Tech Ventures (ATV) INC. will option UML 15-32 IP and explore its commercialization.

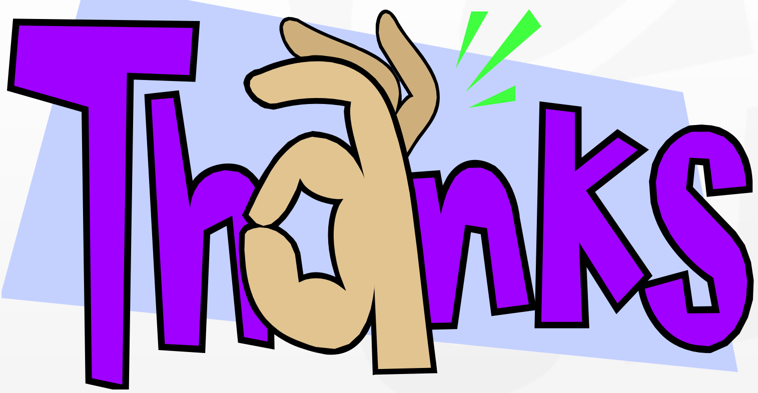
Thanks